Robotica (2022), **40**, pp. 475–504
doi:10.1017/S026357472100062X

CAMBRIDGE
UNIVERSITY PRESS

RESEARCH ARTICLE

Task-based torque minimization of a 3-PRR spherical parallel manipulator

Soheil Zarkandi

Department of Mechanical Engineering, Babol Noshirvani University of Technology, Babol, Iran
Email: zarkandi@gmail.com

Received: 19 November 2020; **Revised:** 1 May 2021; **Accepted:** 2 May 2021; **First published online:** 7 June 2021

Keywords: spherical parallel manipulator; dynamic modeling; Newton-Euler method; SimMechanics; Rzeppa joint; Torque minimization; dynamic dexterity

Abstract

A comprehensive dynamic modeling and actuator torque minimization of a new symmetrical three-degree-of-freedom (3-DOF) 3-PRR spherical parallel manipulator (SPM) is presented. Three actuating systems, each of which composed of an electromotor, a gearbox and a double Rzeppa-type driveshaft, produce input torques of the manipulator. Kinematics of the 3-PRR SPM was recently studied by the author (Zarkandi, *Proc. Inst. Mech. Eng. Part C J. Mech. Eng. Sci.* 2020, https://doi.org/10.1177%2F0954406220938806). In this paper, a closed-form dynamic equation of the manipulator is derived with the Newton–Euler approach. Then, an optimization problem with kinematic and dynamic constraints is presented to minimize torques of the actuators for implementing a given task. The results are also verified by the SimMechanics model of the manipulator.

1. Introduction

Due to the direct proportional relationship between joint torques/forces of a manipulator and its consumed energy, minimizing the torques/forces required for a task would inevitably reduce the power consumption of the manipulator. For this reason, some scholars have addressed torque/force minimization of robot manipulators. The main approaches are (i) trajectory planning of the manipulator [2, 3, 4], (ii) actuation or kinematic redundancy [2, 5, 6, 7]. For instance, Park et al. [2] proposed an optimization procedure to optimize both the end-effector trajectory and actuating torque distribution of a 2-DOF redundantly actuated parallel mechanism. Segota et al. [3] studied torque minimization of a two 6-DOF robotic manipulators cooperating and carrying a weight in a point-to-point trajectory using evolutionary algorithms. Yao et al. [6] added a drive to change the passive constraint branch of a 5UPS/PRPU parallel manipulator into the redundant actuation branch and optimizes the driving torque of the parallel manipulator. The letters R, P, U and S denote a revolute joint, a prismatic joint, a universal joint and a spherical joint, respectively, and underline denotes an actuated joint. They showed that adding the redundant actuation branch can reduce the peak value of other non-redundant branch driving forces and improve its dynamic performance. Boudreau et al. [7] developed an optimization approach to minimize the actuator torques of a 3-PRPR planar parallel manipulator when following a specified trajectory and proved that the redundant manipulator requires smaller torques compared with those of the non-redundant counterpart.

Several three-degree-of-freedom (3-DOF) spherical parallel manipulators (SPMs) have been proposed and their mechanical properties have been studied before; see for instance [1, 8, 9, 10, 11, 12, 13, 14, 15, 16, 17, 18, 19, 20]. But, in the case of torque minimization of 3-DOF SPMs, the literature is so limited. To the best knowledge of the author, the only work that addressed this issue was presented by

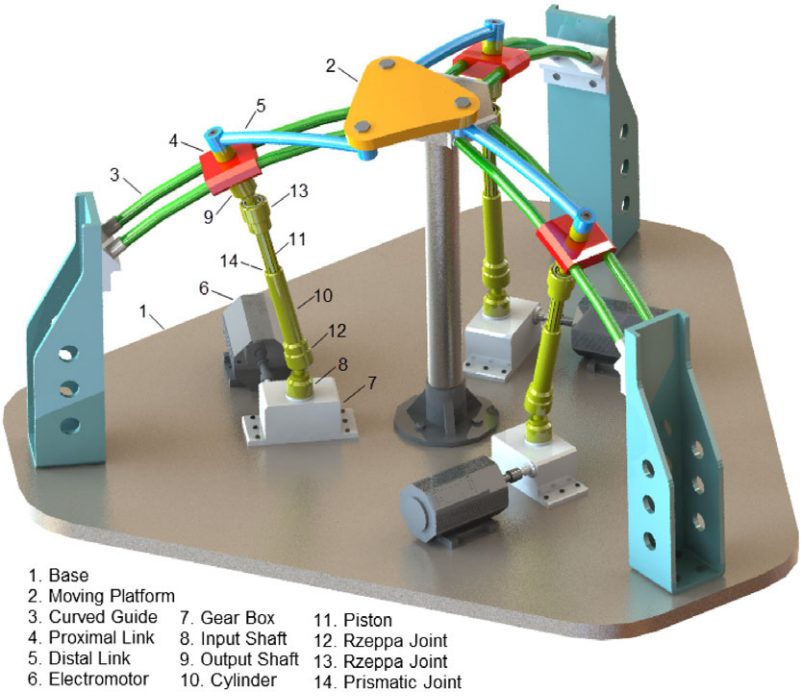

Figure 1. *A 3D CAD model of the star-shaped base 3-PRR SPM.*

Saafi et al. [5] in which an optimal torque distribution approach is studied for a redundant 3-RRR SPM with haptic capabilities.

Dynamic modeling (or dynamic analysis) plays an important role in investigating mechanical behavior of parallel manipulators. The result of the dynamic analysis can be applied for computer simulations, calculating joint reaction forces and moments, sizing links, selecting bearings and actuators, vibration analysis, motion planning and real-time control strategies. Dynamic analysis of parallel manipulators has two branches [12]: (i) the inverse dynamic analysis in which the desired trajectory of the moving platform and the mass distribution of each link is given, and the aim is to find actuator torques to generate the trajectory and (ii) the forward (or direct) dynamic analysis in which initial actuated joint positions and velocities, applied actuated torques, applied external forces to the moving platform are given, and the aim is to find the resulting motion of the moving platform.

Many methods have been proposed to formulate dynamic equation of parallel manipulators such as the Newton-Euler method [21, 22], principle of virtual work [9, 10, 11, 12], Euler-Lagrange method [24], Kane's method [19, 25] and some other methods [26, 27, 28]. Essentially, all the methods for obtaining dynamic equations of motion have their own advantages and disadvantages [23]. The ease of use of the various methods differs and depends on the type and complexity of the manipulator structure.

A small number of works have been done on dynamic analysis of 3-DOF SPMs, and most of them are based on the principle of virtual work [9, 10, 11, 12]. Staicu [9, 10] analyzed the inverse dynamics of 3-RRR (or Agile wrist) and 3UPS+S SPMs using the virtual work principle and recursive matrix relations. Akbarzadeh et al. [11, 12] used the virtual work principle and the concept of link Jacobian matrices for the inverse and direct dynamic analyses of a Star-Triangle SPM.

A novel 3-PRR SPM was recently introduced by the author [1], and its kinematics and workspace were analyzed in detail. A 3D CAD model of the 3-PRR SPM is shown in Fig. 1. The manipulator has a symmetrical architecture with an equiangular star-shaped base and an equilateral triangle-shaped moving platform. Three identical PRR legs connect the base to the moving platform. The base itself consists of three curved guides on which proximal links of the PRR legs move freely through curved

https://doi.org/10.1017/S026357472100062X Published online by Cambridge University Press

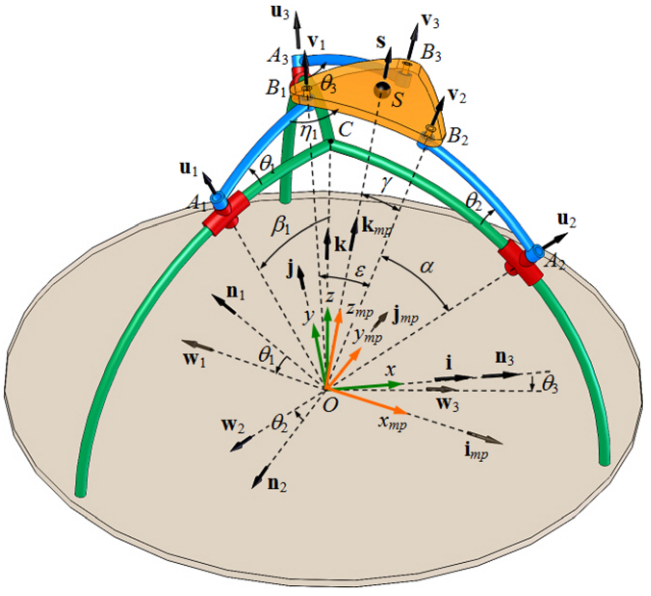

Figure 2. *Kinematic model and unit vectors of the star-shaped base 3-PRR SPM.*

prismatic joints. Distal links of the PRR legs are connected to the proximal links via revolute joints. Each of these revolute joints is actuated by an actuating system having an electromotor fixed to the base, a gearbox and a double Rzeppa-type driveshaft [1]. The driveshaft is composed of an input shaft, an output shaft and two intermediate shafts (a cylinder and a piston) connected to each other through two Rzeppa joints and a prismatic joint.

The 3-PRR SPM has closed-form solutions for the inverse and forward position kinematics problems, leading to eight working modes and eight assembly modes, respectively [1]. In contrast to the traditional 3-DOF SPM with 3-RRR topology [8, 18, 20, 29] in which all the joints are of revolute (R) type and the first R joint of each leg is actuated, in the 3-PRR SPM, the first joint of each leg is a curved prismatic (P) joint, and not actuated. This especial structure admits several superiorities of the 3-PRR SPM; for instance, it has no forward kinematic singularity in its workspace for a wide range of rotation of the moving platform around its central axis. Moreover, the uniquely acceptable working and assembly modes of the manipulator can be easily tracked during its motion [1].

The main contribution of this paper is actuator torque minimization of the 3-PRR SPM for a given task. To this aim, first, a complete dynamic modeling of the manipulator is developed via the Newton-Euler method, and actuator torques of the manipulator are calculated. Then, through a constrained optimization problem, an optimum design of the manipulator is determined with minimum values of actuator torques required for the task.

2. Description of the 3-PRR SPM and notations

A kinematic model of the symmetrical 3-PRR SPM is represented in Fig. 2. Three curved guides of the star-shaped base located on the surface of a sphere. The guides are concurrent at point C, and the angle between them is $2\pi/3$. Throughout this paper, we take subscript $i = 1, 2, 3$ in a cyclic manner. Subscripts "*mp*" refers to the moving platform, subscripts "*pro*,*i*" and "*dis*,*i*" refer to the proximal link and distal link of the ith PRR leg, and subscripts "*cyl*,*i*", "*pis*,*i*" and "*sh*,*i*" refer to the piston, cylinder and intermediate shafts of the ith driveshaft, respectively. Point A_i (B_i) locates at the intersection of the axis of actuated (passive) revolute joint of the distal link A_iB_i and central arc of the curved solid bar of the same link, see Fig. 6. It is assumed that the moving platform, the proximal link and the distal link of

https://doi.org/10.1017/S026357472100062X Published online by Cambridge University Press

the *i*th PRR leg move on the surface of three concentric spheres. Centers of these spheres are coincident with the center of the sphere of the star-shaped base at point *O*. The *i*th proximal link rotates around the unit vector normal to the plane of the *i*th curved guide, which is given as

$$\mathbf{n}_i = [\cos\psi_i \quad \sin\psi_i \quad 0]^T \tag{1}$$

where $\psi_1 = 2\pi/3$, $\psi_2 = -2\pi/3$ and $\psi_3 = 0$. Rotation of the *i*th proximal link around $\mathbf{n}_i$ is given by angle $\beta_i \in [0, \beta_{max}]$ which is the angle from $\mathbf{k}$ to $\mathbf{u}_i$. Two unit vectors $\mathbf{u}_i = [u_{ix}\ u_{iy}\ u_{iz}]^T$ and $\mathbf{v}_i = [v_{ix}\ v_{iy}\ v_{iz}]^T$ represent rotation axes of the first and the second revolute joints at A_i and B_i, respectively. Unit vector $\mathbf{w}_i = [w_{ix}, w_{iy}, w_{iz}]^T$ is perpendicular to the plane passing through vectors $\mathbf{u}_i$ and $\mathbf{v}_i$. The angle between $\mathbf{u}_i$ and $\mathbf{v}_i$ of the *i*th distal link is shown by α. Angle θ_i is the rotation angle of the actuated revolute joint at A_i, and is the angle from $\mathbf{n}_i$ to $\mathbf{w}_i$ around $\mathbf{u}_i$. Angle η_i is the rotation angle of the second revolute joint at B_i and is equal to the angle from the plane passing through $\mathbf{u}_i$ and $\mathbf{v}_i$ to the plane passing through $\mathbf{v}_i$ and $\mathbf{v}_{i+1}$ modulo 3 [1]. The angles β_i, θ_i and η_i are taken positive if measured counterclockwise around $\mathbf{n}_i$, $\mathbf{u}_i$ and $\mathbf{v}_i$, respectively.

The central point *S* of the moving platform is chosen as its operating point. Unit vector $\mathbf{s} = [s_x\ s_y\ s_z]^T$ is along $\overrightarrow{OS}$. Angle γ of the moving platform is the angle between $\mathbf{s}$ and $\mathbf{v}_i$.

A fixed coordinate frame *O*-*xyz* is attached at the centered point *O*, while its *z*-axis is along the vector $\overrightarrow{OC}$, and its *y*-axis locates in the plane passing through the arc of the third curved guide and point *O*. Three unit vectors $\mathbf{i}$, $\mathbf{j}$ and $\mathbf{k}$ are considered along the *x*, *y* and *z* axes, respectively. All the above unit vectors pass through the center of rotation, that is, point *O*, of the manipulator.

The author [1] showed that the inverse position kinematics of the 3-PRR SPM leads to two solutions (or working modes) for θ_i, while the orientation of the moving platform is known. On the other hand, the forward position kinematics of the manipulator gives eight solutions (or assembly modes) for the orientation of the moving platform, when the rotation angles θ_i are given. Two simple techniques were also presented in ref. [1] to find unique and acceptable working and assembly modes of the 3-PRR SPM. Therefore, unique postures of the manipulator can be easily traced during its motion.

3. Local coordinates frames and rotation matrices of the moving links

A local coordinate frame $O{-}x_{mp}y_{mp}z_{mp}$ is attached to the moving platform (Fig. 2), whose z_{mp} axis is along a vector $\overrightarrow{OS}$, and the y_{mp} axis locates in the plane passing through $\mathbf{s}$ and $\mathbf{v}_3$. Three unit vectors $\mathbf{i}_{mp}$, $\mathbf{j}_{mp}$ and $\mathbf{k}_{mp}$ are defined along the x_{mp}, y_{mp} and z_{mp} axes, respectively; thus $\mathbf{s} \equiv \mathbf{k}_{mp}$. Pose of the moving platform with respect to the base coordinate frame *O*-*xyz* is completely determined by three successive rotation angles (or Euler angles[30]) φ_x, φ_y and φ_z around the fixed *x*, *y* and *z* axes, respectively, while φ_x, $\varphi_z \in (-\pi, \pi]$ and $\varphi_y \in [-\pi/2, \pi/2]$. Therefore, the rotation matrix of the moving platform with respect to the base platform will be formed by multiplying the corresponding rotation matrices as follows:

$$\mathbf{R}_{mp} = \begin{bmatrix} c\varphi_z c\varphi_y & c\varphi_z s\varphi_y s\varphi_x - s\varphi_z c\varphi_x & c\varphi_z s\varphi_y c\varphi_x + s\varphi_z s\varphi_x \\ s\varphi_z c\varphi_y & s\varphi_z s\varphi_y s\varphi_x + c\varphi_z c\varphi_x & s\varphi_z s\varphi_y c\varphi_x - c\varphi_z s\varphi_x \\ -s\varphi_y & c\varphi_y s\varphi_x & c\varphi_y c\varphi_x \end{bmatrix} \tag{2}$$

where *c*(.) and *s*(.) stand for *cos*(.) and *sin*(.), respectively. We can also define the rotation matrix of the moving platform based on unit vectors $\mathbf{i}_{mp}$, $\mathbf{j}_{mp}$ and $\mathbf{k}_{mp}$ as follows:

$$\mathbf{R}_{mp} = [\mathbf{i}_{mp} \quad \mathbf{j}_{mp} \quad \mathbf{k}_{mp}]^T \tag{3}$$

As a result, the first, the second and the third columns of $\mathbf{R}_{mp}$ in Eq. (2) represent unit vectors $\mathbf{i}_{mp}$, $\mathbf{j}_{mp}$ and $\mathbf{k}_{mp}$ respectively.

Two additional coordinate frames $O{-}x_{pro,i}y_{pro,i}z_{pro,i}$ and $O{-}x_{dis,i}y_{dis,i}z_{dis,i}$ are defined for the proximal and distal links of *i*th PRR leg of the manipulator, respectively (Fig. 3). In the coordinate frame $O{-}x_{pro,i}y_{pro,i}z_{pro,i}$, the $z_{pro,i}$ and $x_{pro,i}$ axes are along $\mathbf{u}_i$ and $\mathbf{n}_i$, respectively. In the coordinate frame

https://doi.org/10.1017/S026357472100062X Published online by Cambridge University Press

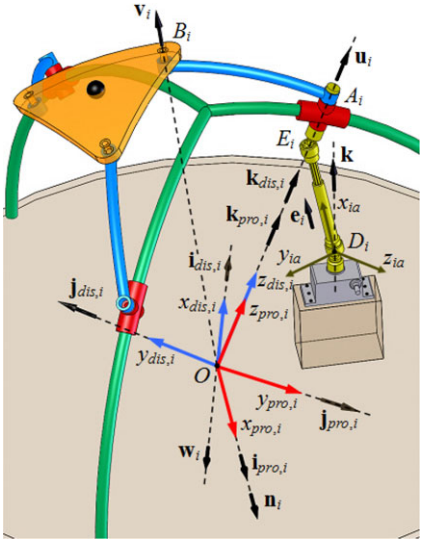

Figure 3. *Local coordinate frames and unit vectors of the ith kinematic chain of the 3-PRR SPM.*

O−$x_{dis,i}y_{dis,i}z_{dis,i}$, the $z_{dis,i}$ and $x_{dis,i}$ axes are along $\mathbf{u}_i$ and $-\mathbf{w}_i$, respectively. The $y_{pro,i}$ and $y_{dis,i}$ axes are determined by the right-hand rule. Three unit vectors $\mathbf{i}_{pro,i}$ ($\mathbf{i}_{dis,i}$), $\mathbf{j}_{pro,i}$ ($\mathbf{j}_{dis,i}$) and $\mathbf{k}_{pro,i}$ ($\mathbf{k}_{dis,i}$) are considered along the $x_{pro,i}$ ($x_{dis,i}$), $y_{pro,i}$ ($y_{dis,i}$) and $z_{pro,i}$ ($z_{dis,i}$) axes, respectively.

Using coordinate frames O−$x_{pro,i}y_{pro,i}z_{pro,i}$ and O−$x_{dis,i}y_{dis,i}z_{dis,i}$, the 3×3 rotation matrices of proximal link and distal link of the ith PRR leg are defined respectively as

$$\mathbf{R}_{pro,i} = \begin{bmatrix}\mathbf{i}_{pro,i} & \mathbf{j}_{pro,i} & \mathbf{k}_{pro,i}\end{bmatrix} = [\mathbf{n}_i \quad \mathbf{u}_i \times \mathbf{n}_i \quad \mathbf{u}_i] \tag{4a}$$

$$\mathbf{R}_{dis,i} = \begin{bmatrix}\mathbf{i}_{dis,i} & \mathbf{j}_{dis,i} & \mathbf{k}_{dis,i}\end{bmatrix} = [-\mathbf{w}_i \quad \mathbf{w}_i \times \mathbf{u}_i \quad \mathbf{u}_i] \tag{4b}$$

The ith double Rzeppa-type driveshaft is also shown in Fig. 3. The Rzeppa joints locate at points D_i and E_i. The axis of input (output) shaft of the driveshaft is parallel to $\mathbf{k}$ ($\mathbf{u}_i$). Unit vector $\mathbf{e}_i = [e_{ix}\ e_{iy}\ e_{iz}]^T$ is along the common axis of the cylinder and piston of the ith driveshaft. For the ith double Rzeppa-type driveshaft, a local coordinate frame D_i−$x_{ia}y_{ia}z_{ia}$ is attached at point D_i (Fig. 3), while the x_{ia} axis is along the vector $\mathbf{e}_i$, y_{ia} axis is along the vector $\mathbf{e}_i \times \mathbf{k}$, and the z_{ia} axis is determined by the right-hand rule. Since the cylinder and piston of the ith driveshaft has no rotational motion with respect to each other, we can define a common rotation matrix for these two links, as follows:

$$\mathbf{R}_{sh,i} = \begin{bmatrix}\mathbf{e}_i & \dfrac{\mathbf{e}_i \times \mathbf{k}}{\|\mathbf{e}_i \times \mathbf{k}\|} & \dfrac{\mathbf{e}_i \times (\mathbf{e}_i \times \mathbf{k})}{\|\mathbf{k} \times (\mathbf{e}_i \times \mathbf{k})\|}\end{bmatrix} \tag{5}$$

Using the above rotation matrices, positions of mass centers of the moving platform (c_{mp}) and the proximal link ($c_{pro,i}$) and distal link ($c_{dis,i}$) of the ith PRR leg (Fig. 4) are determined respectively as

$$\mathbf{r}_{mp} = \overrightarrow{Oc_{mp}} = \mathbf{R}_{mp}\bar{\mathbf{r}}_{mp} \tag{6a}$$

$$\mathbf{r}_{pro,i} = \overrightarrow{Oc_{pro,i}} = \mathbf{R}_{pro,i}\bar{\mathbf{r}}_{pro} \tag{6b}$$

$$\mathbf{r}_{dis,i} = \overrightarrow{Oc_{dis,i}} = \mathbf{R}_{dis,i}\bar{\mathbf{r}}_{dis} \tag{6c}$$

where $\bar{\mathbf{r}}_{mp}$, $\bar{\mathbf{r}}_{pro}$ and $\bar{\mathbf{r}}_{dis}$ are position vectors of mass centers of the moving platform, proximal links and distal links in the local coordinate frames O−$x_{mp}y_{mp}z_{mp}$, O−$x_{pro,i}y_{pro,i}z_{pro,i}$ and O−$x_{dis,i}y_{dis,i}z_{dis,i}$, respectively.

https://doi.org/10.1017/S026357472100062X Published online by Cambridge University Press

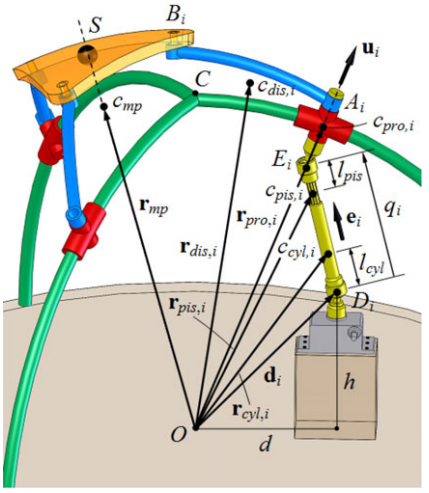

Figure 4. *Mass centers of the moving platform, the ith proximal and distal links and of the ith actuating system.*

Positions of mass centers of the cylinder and piston of the *i*th double Rzeppa-type driveshaft (Fig. 4) are obtained by the following relations, respectively:

$$\mathbf{r}_{cyl,i} = \overrightarrow{Oc_{cyl,i}} = \mathbf{d}_i + l_{cyl}\mathbf{e}_i \tag{7a}$$

$$\mathbf{r}_{pis,i} = \overrightarrow{Oc_{pis,i}} = \boldsymbol{\delta}_i - l_{pis}\mathbf{e}_i \tag{7b}$$

where $\mathbf{d}_i = [d_{ix}\ d_{iy}\ d_{iz}]^T$ and $\boldsymbol{\delta}_i = [\delta_{ix}\ \delta_{iy}\ \delta_{iz}]^T$ are

$$\mathbf{d}_i = \overrightarrow{OD_i} = [-d\sin\psi_i \quad d\cos\psi_i \quad h]^T \tag{8a}$$

$$\boldsymbol{\delta}_i = \overrightarrow{OE_i} = \mathbf{r}_{pro,i} - \overline{E_i c_{pro,i}}\mathbf{u}_i \tag{8b}$$

and l_{cyl} (l_{pis}) is the distance between point D_i (E_i) and mass center $c_{cyl,i}$ ($c_{pis,i}$). Stroke of prismatic joint of the *i*th driveshaft is represented by $q_i = \left\|\overrightarrow{D_iE_i}\right\|$, and unit vector $\mathbf{e}_i$ is given as

$$\mathbf{e}_i = \frac{\overrightarrow{D_iE_i}}{\left\|\overrightarrow{D_iE_i}\right\|} = \frac{\boldsymbol{\delta}_i - \mathbf{d}_i}{\|\boldsymbol{\delta}_i - \mathbf{d}_i\|} \tag{9}$$

4. Velocity analysis and jacobian matrices

4.1. Jacobian matrices of the manipulator

Referring to Fig. 2, the angular velocity of the moving platform, $\boldsymbol{\omega}_{mp}$, can be calculated through angular velocities of links of the *i*th PRR leg, as follows:

$$\mathbf{n}_i\dot{\beta}_i + \mathbf{u}_i\dot{\theta}_i + \mathbf{v}_i\dot{\eta}_i = \boldsymbol{\omega}_{mp} \tag{10}$$

Dot multiplying both sides of Eq. (10) by $\mathbf{n}_i \times \mathbf{v}_i$ and rearranging the resultant equation gives

$$\mathbf{n}_i^T(\mathbf{u}_i \times \mathbf{v}_i)\dot{\theta}_i + (\mathbf{n}_i \times \mathbf{v}_i)^T\boldsymbol{\omega}_{mp} = 0 \tag{11}$$

Writing Eq. (11) for $i = 1, 2, 3$, and assembling the resultant equations into a matrix form yields

$$\mathbf{J}_{inv}\dot{\boldsymbol{\theta}} + \mathbf{J}_{fwd}\boldsymbol{\omega}_{mp} = \mathbf{0} \tag{12}$$

https://doi.org/10.1017/S026357472100062X Published online by Cambridge University Press

where $\dot{\boldsymbol{\theta}} = [\,\dot{\theta}_1 \quad \dot{\theta}_2 \quad \dot{\theta}_3\,]^T$ is the velocity vector of the actuated joints, and $\mathbf{J}_{inv}$ and $\mathbf{J}_{fwd}$ are the inverse and forward Jacobian matrices of the 3-PRR SPM, respectively, as follows [1]:

$$\mathbf{J}_{inv} = \begin{bmatrix} \mathbf{n}_1^T(\mathbf{u}_1 \times \mathbf{v}_1) & 0 & 0 \\ 0 & \mathbf{n}_2^T(\mathbf{u}_2 \times \mathbf{v}_2) & 0 \\ 0 & 0 & \mathbf{n}_3^T(\mathbf{u}_3 \times \mathbf{v}_3) \end{bmatrix} \tag{13}$$

$$\mathbf{J}_{fwd} = \begin{bmatrix} (\mathbf{n}_1 \times \mathbf{v}_1)^T \\ (\mathbf{n}_2 \times \mathbf{v}_2)^T \\ (\mathbf{n}_3 \times \mathbf{v}_3)^T \end{bmatrix} \tag{14}$$

4.2. Jacobian matrix of the moving platform

To find the Jacobian matrix, $\mathbf{J}_{mp}$, of the moving platform, Eq. (12) is rewritten as

$$\boldsymbol{\omega}_{mp} = \mathbf{J}_{mp}\dot{\boldsymbol{\theta}} \tag{15}$$

where

$$\mathbf{J}_{mp} = -\mathbf{J}_{fwd}^{-1}\mathbf{J}_{inv} \tag{16}$$

4.3. Jacobian matrices of the ith PRR leg

For the proximal link of the ith PRR leg, first, the parameter $\dot{\beta}_i$ is calculated through dot multiplying both sides of Eq. (10) by $\mathbf{u}_i \times \mathbf{v}_i$, which gives

$$\mathbf{n}_i^T(\mathbf{u}_i \times \mathbf{v}_i)\dot{\beta}_i = (\mathbf{u}_i \times \mathbf{v}_i)^T\boldsymbol{\omega}_{mp} \tag{17}$$

Therefore

$$\dot{\beta}_i = \frac{(\mathbf{u}_i \times \mathbf{v}_i)^T\boldsymbol{\omega}_{mp}}{\mathbf{n}_i^T(\mathbf{u}_i \times \mathbf{v}_i)} \tag{18}$$

The ith proximal link rotates about unit vector $\mathbf{n}_i$, so its angular velocity can be expressed as

$$\boldsymbol{\omega}_{pro,i} = \mathbf{n}_i\dot{\beta}_i \tag{19}$$

Introducing $\dot{\beta}_i$ and $\boldsymbol{\omega}_{mp}$ from Eqs. (18) and (15) into Eq. (19), and doing some manipulations, yields

$$\boldsymbol{\omega}_{pro,i} = \mathbf{J}_{pro,i}\dot{\boldsymbol{\theta}} \tag{20}$$

where $\mathbf{J}_{pro,i}$ is the 3×3 link Jacobian matrix of the proximal link of the ith PRR leg, as

$$\mathbf{J}_{pro,i} = \frac{1}{\mathbf{n}_i^T(\mathbf{u}_i \times \mathbf{v}_i)} \begin{bmatrix} n_{ix}(\mathbf{u}_i \times \mathbf{v}_i)^T\mathbf{J}_{mp} \\ n_{iy}(\mathbf{u}_i \times \mathbf{v}_i)^T\mathbf{J}_{mp} \\ n_{iz}(\mathbf{u}_i \times \mathbf{v}_i)^T\mathbf{J}_{mp} \end{bmatrix} \tag{21}$$

The ith distal link rotates about unit vector $\mathbf{u}_i$, and its angular velocity can be expressed by

$$\boldsymbol{\omega}_{dis,i} = \boldsymbol{\omega}_{pro,i} + \mathbf{u}_i\dot{\theta}_i \tag{22}$$

Introducing $\boldsymbol{\omega}_{pro,i}$ from Eq. (20) into Eq. (22) yields

$$\boldsymbol{\omega}_{dis,i} = \mathbf{J}_{dis,i}\dot{\boldsymbol{\theta}} \tag{23}$$

https://doi.org/10.1017/S026357472100062X Published online by Cambridge University Press

where $\mathbf{J}_{dis,i}$ is the 3×3 link Jacobian matrix of the distal link of the ith PRR leg, as

$$\mathbf{J}_{dis,i} = \mathbf{J}_{pro,i} + \begin{bmatrix} u_{ix}\mathbf{1}_{i\times(1-3)} \\ u_{iy}\mathbf{1}_{i\times(1-3)} \\ u_{iz}\mathbf{1}_{i\times(1-3)} \end{bmatrix} \tag{24}$$

and $\mathbf{1}_{i\times(1-3)}$ denotes the ith row of 3×3 identity matrix $\mathbf{1}_{3\times 3}$.

4.4. Jacobian matrix of the ith intermediate shafts

The cylinder and piston of the ith driveshaft (Fig. 4) have a relative translational motion with velocity $\dot{q}_i\mathbf{e}_i$. They also have two common rotational motions, one of which is around point D_i with angular velocity $\boldsymbol{\omega}_i$ and another one is around the axis of the ith driveshaft with angular velocity $\dot{\theta}_i\mathbf{e}_i$.

The velocity of point E_i can be obtained in terms of velocities of the ith proximal link and of the ith driveshaft, as follows:

$$\mathbf{v}_{Ei} = \boldsymbol{\omega}_{pro,i} \times \boldsymbol{\delta}_i \tag{25}$$

$$\mathbf{v}_{Ei} = q_i\boldsymbol{\omega}_i \times \mathbf{e}_i + \dot{q}_i\mathbf{e}_i \tag{26}$$

Equating right-hand sides of Eqs. (25) and (26), and then substituting $\boldsymbol{\omega}_{pro,i}$ from Eq. (20) into the resultant equation results in

$$\mathbf{J}_{pro,i}\dot{\boldsymbol{\theta}} \times \boldsymbol{\delta}_i = q_i\boldsymbol{\omega}_i \times \mathbf{e}_i + \dot{q}_i\mathbf{e}_i \tag{27}$$

Since $\boldsymbol{\omega}_i$ has no component along the axis of the shaft, we have $\mathbf{e}_i \times (\boldsymbol{\omega}_i \times \mathbf{e}_i) = \boldsymbol{\omega}_i$, and cross multiplying both sides of Eq. (27) by $\mathbf{e}_i$ yields

$$\boldsymbol{\omega}_i = (1/q_i)(\mathbf{e}_i \times (\mathbf{J}_{pro,i}\dot{\boldsymbol{\theta}} \times \boldsymbol{\delta}_i)) \tag{28}$$

From linear algebra, we know that

$$\mathbf{a} \times (\mathbf{b} \times \mathbf{c}) = (\mathbf{a}^T\mathbf{c})\mathbf{b} - (\mathbf{a}^T\mathbf{b})\mathbf{c} \tag{29}$$

Considering relation (29), we can rewrite Eq. (28) as follows:

$$\boldsymbol{\omega}_i = (1/q_i)((\mathbf{e}_i^T\boldsymbol{\delta}_i)\mathbf{J}_{pro,i}\dot{\boldsymbol{\theta}} - (\mathbf{e}_i^T\mathbf{J}_{pro,i}\dot{\boldsymbol{\theta}})\boldsymbol{\delta}_i) \tag{30}$$

or

$$\boldsymbol{\omega}_i = \mathbf{J}_{\omega i}\dot{\boldsymbol{\theta}} \tag{31}$$

where

$$\mathbf{J}_{\omega i} = (1/q_i)(\mathbf{e}_i^T\boldsymbol{\delta}_i)\mathbf{J}_{pro,i} - (1/q_i)\begin{bmatrix} \mathbf{e}_i^T\mathbf{J}_{pro,i}\delta_{ix} \\ \mathbf{e}_i^T\mathbf{J}_{pro,i}\delta_{iy} \\ \mathbf{e}_i^T\mathbf{J}_{pro,i}\delta_{iz} \end{bmatrix} \tag{32}$$

The total angular velocity of the ith intermediate shafts is determined as

$$\boldsymbol{\omega}_{sh,i} = \boldsymbol{\omega}_i + \dot{\theta}_i\mathbf{e}_i \tag{33}$$

Substituting $\boldsymbol{\omega}_i$ from Eq. (31) into Eq. (33) results in

$$\boldsymbol{\omega}_{sh,i} = \mathbf{J}_{sh,i}\dot{\boldsymbol{\theta}} \tag{34}$$

where

$$\mathbf{J}_{sh,i} = \mathbf{J}_{\omega i} + \begin{bmatrix} e_{ix}\mathbf{1}_{i\times(1-3)} \\ e_{iy}\mathbf{1}_{i\times(1-3)} \\ e_{iz}\mathbf{1}_{i\times(1-3)} \end{bmatrix} \tag{35}$$

https://doi.org/10.1017/S026357472100062X Published online by Cambridge University Press

Equation (33) can be rewritten for the cylinder and piston of the ith driveshaft as

$$\boldsymbol{\omega}_{cyl,i} = \mathbf{J}_{cyl,i}\dot{\boldsymbol{\theta}} \tag{36a}$$

$$\boldsymbol{\omega}_{pis,i} = \mathbf{J}_{pis,i}\dot{\boldsymbol{\theta}} \tag{36b}$$

where

$$\mathbf{J}_{cyl,i} = \mathbf{J}_{pis,i} = \mathbf{J}_{sh,i} \tag{37}$$

5. Acceleration analysis

In acceleration analysis of the 3-PRR SPM, the relations between angular accelerations of the moving links and acceleration of actuated joints $\ddot{\boldsymbol{\theta}} = [\,\ddot{\theta}_1 \quad \ddot{\theta}_2 \quad \ddot{\theta}_3\,]^T$ are determined.

5.1. Angular acceleration of the moving platform

Differentiating both sides of Eq. (10) with respect to time yields

$$\mathbf{n}_i\ddot{\beta}_i + \mathbf{u}_i\ddot{\theta}_i + \mathbf{n}_i\dot{\beta}_i \times \mathbf{u}_i\dot{\theta}_i + \mathbf{v}_i\ddot{\eta}_i + \mathbf{u}_i\dot{\theta}_i \times \mathbf{v}_i\dot{\eta}_i = \dot{\boldsymbol{\omega}}_{mp} \tag{38}$$

To eliminate angular accelerations of the passive curved prismatic joint and the passive revolute joint, that is $\ddot{\beta}_i$ and $\ddot{\eta}_i$, both sides of Eq. (38) are dot multiplied by $\mathbf{n}_i \times \mathbf{v}_i$, which simplifies to

$$\mathbf{u}_i^T(\mathbf{n}_i \times \mathbf{v}_i)\ddot{\theta}_i + (\mathbf{n}_i \times \mathbf{u}_i)^T(\mathbf{n}_i \times \mathbf{v}_i)\dot{\beta}_i\dot{\theta}_i + (\mathbf{u}_i \times \mathbf{v}_i)^T(\mathbf{n}_i \times \mathbf{v}_i)\dot{\theta}_i\dot{\eta}_i = \dot{\boldsymbol{\omega}}_{mp}^T(\mathbf{n}_i \times \mathbf{v}_i) \tag{39}$$

To obtain the passive joint rate $\dot{\eta}_i$, both sides of Eq. (10) is dot multiplied by $\mathbf{n}_i \times \mathbf{u}_i$, as

$$\mathbf{v}_i^T(\mathbf{n}_i \times \mathbf{u}_i)\dot{\eta}_i = \boldsymbol{\omega}_{mp}^T(\mathbf{n}_i \times \mathbf{u}_i) \tag{40}$$

Therefore

$$\dot{\eta}_i = \frac{(\mathbf{n}_i \times \mathbf{u}_i)^T\boldsymbol{\omega}_{mp}}{(\mathbf{n}_i \times \mathbf{u}_i)^T\mathbf{v}_i} \tag{41}$$

Substituting $\dot{\eta}_i$, $\dot{\beta}_i$ and $\boldsymbol{\omega}_{mp}$ from Eqs. (41), (18) and (15) into Eq. (39) and writing the resultant equation for i = 1, 2, 3, leads to the acceleration equation of the manipulator as follows:

$$\mathbf{J}_{inv}\ddot{\boldsymbol{\theta}} + \boldsymbol{\Omega}\dot{\boldsymbol{\theta}} + \mathbf{J}_{fwd}\dot{\boldsymbol{\omega}}_{mp} = \mathbf{0} \tag{42}$$

where

$$\boldsymbol{\Omega} = \begin{bmatrix} \Omega_1 & 0 & 0 \\ 0 & \Omega_2 & 0 \\ 0 & 0 & \Omega_3 \end{bmatrix} \tag{43}$$

with

$$\Omega_i = -\frac{((\mathbf{u}_i \times \mathbf{v}_i)^T\mathbf{J}_{mp}\dot{\boldsymbol{\theta}}(\mathbf{n}_i \times \mathbf{u}_i) + (\mathbf{n}_i \times \mathbf{u}_i)^T\mathbf{J}_{mp}\dot{\boldsymbol{\theta}}(\mathbf{u}_i \times \mathbf{v}_i))^T(\mathbf{n}_i \times \mathbf{v}_i)}{\mathbf{n}_i^T(\mathbf{u}_i \times \mathbf{v}_i)} \tag{44}$$

Therefore, the angular acceleration of the moving platform is obtained in terms of $\dot{\boldsymbol{\theta}}$ and $\ddot{\boldsymbol{\theta}}$, as follows:

$$\dot{\boldsymbol{\omega}}_{mp} = \mathbf{J}_{\dot{\omega},mp,1}\ddot{\boldsymbol{\theta}} + \mathbf{J}_{\dot{\omega},mp,2}\dot{\boldsymbol{\theta}} \tag{45}$$

where

$$\mathbf{J}_{\dot{\omega},mp,1} = \mathbf{J}_{mp} \tag{46a}$$

$$\mathbf{J}_{\dot{\omega},mp,2} = -\mathbf{J}_{fwd}^{-1}\boldsymbol{\Omega} \tag{46b}$$

https://doi.org/10.1017/S026357472100062X Published online by Cambridge University Press

5.2. Angular accelerations of proximal and distal links of the ith PRR leg

To calculate $\ddot{\beta}_i$, both sides of Eq. (38) is dot multiplied by $\mathbf{u}_i \times \mathbf{v}_i$, which gives

$$(\mathbf{u}_i \times \mathbf{v}_i)^T \mathbf{n}_i \ddot{\beta}_i + (\mathbf{u}_i \times \mathbf{v}_i)^T (\mathbf{n}_i \times \mathbf{u}_i) \dot{\beta}_i \dot{\theta}_i + \dot{\theta}_i \dot{\eta}_i = (\mathbf{u}_i \times \mathbf{v}_i)^T \dot{\boldsymbol{\omega}}_{mp} \tag{47}$$

Thus

$$\ddot{\beta}_i = \frac{(\mathbf{u}_i \times \mathbf{v}_i)^T \dot{\boldsymbol{\omega}}_{mp}}{(\mathbf{u}_i \times \mathbf{v}_i)^T \mathbf{n}_i} - \frac{(\mathbf{u}_i \times \mathbf{v}_i)^T (\mathbf{n}_i \times \mathbf{u}_i)}{(\mathbf{u}_i \times \mathbf{v}_i)^T \mathbf{n}_i} \dot{\beta}_i \dot{\theta}_i - \frac{\dot{\theta}_i \dot{\eta}_i}{(\mathbf{u}_i \times \mathbf{v}_i)^T \mathbf{n}_i} \tag{48}$$

The ith proximal link rotates about unit vector $\mathbf{n}_i$, so its angular acceleration will be

$$\dot{\boldsymbol{\omega}}_{pro,i} = \mathbf{n}_i \ddot{\beta}_i \tag{49}$$

Substituting $\ddot{\beta}_i$ and then $\dot{\beta}_i$, $\dot{\eta}_i$, $\boldsymbol{\omega}_{mp}$ and $\dot{\boldsymbol{\omega}}_{mp}$ from Eqs. (48), (18), (41), (15) and (45) into Eq. (49) and rearranging the resultant equation gives $\dot{\boldsymbol{\omega}}_{pro,i}$ in terms of $\dot{\boldsymbol{\theta}}$ and $\ddot{\boldsymbol{\theta}}$, as follows:

$$\dot{\boldsymbol{\omega}}_{pro,i} = \mathbf{J}_{\dot{\omega},pro,i,1} \ddot{\boldsymbol{\theta}} + \mathbf{J}_{\dot{\omega},pro,i,2} \dot{\boldsymbol{\theta}} \tag{50}$$

where the 3×3 matrices $\mathbf{J}_{\dot{\omega},pro,i,1}$ and $\mathbf{J}_{\dot{\omega},pro,i,2}$ are obtained in Appendix A. The angular acceleration of the ith distal link is obtained as

$$\dot{\boldsymbol{\omega}}_{dis,i} = \dot{\boldsymbol{\omega}}_{pro,i} + \mathbf{u}_i \ddot{\theta}_i \tag{51}$$

Substituting $\dot{\boldsymbol{\omega}}_{pro,i}$ from Eq. (50) into Eq. (51) yields $\dot{\boldsymbol{\omega}}_{dis,i}$ in terms of $\dot{\boldsymbol{\theta}}$ and $\ddot{\boldsymbol{\theta}}$, as follows:

$$\dot{\boldsymbol{\omega}}_{dis,i} = \mathbf{J}_{\dot{\omega},dis,i,1} \ddot{\boldsymbol{\theta}} + \mathbf{J}_{\dot{\omega},dis,i,2} \dot{\boldsymbol{\theta}} \tag{52}$$

where the 3×3 matrices $\mathbf{J}_{\dot{\omega},dis,i,1}$ and $\mathbf{J}_{\dot{\omega},dis,i,2}$ are given respectively by

$$\mathbf{J}_{\dot{\omega},dis,i,1} = \mathbf{J}_{\dot{\omega},pro,i,1} + \begin{bmatrix} u_{ix} \mathbf{1}_{i\times(1-3)} \\ u_{iy} \mathbf{1}_{i\times(1-3)} \\ u_{iz} \mathbf{1}_{i\times(1-3)} \end{bmatrix} \tag{53a}$$

$$\mathbf{J}_{\dot{\omega},dis,i,2} = \mathbf{J}_{\dot{\omega},pro,i,2} \tag{53b}$$

5.3. Angular accelerations of the ith intermediate shafts

Angular accelerations of the cylinder and piston of the ith driveshaft around point D_i and around their common axis are represented by $\dot{\boldsymbol{\omega}}_i$ and $\ddot{\theta}_i \mathbf{e}_i$, respectively. Differentiating Eqs. (25) and (26) with respect to time and equating the resultant equations yields

$$\dot{\boldsymbol{\omega}}_{pro,i} \times \boldsymbol{\delta}_i + \boldsymbol{\omega}_{pro,i} \times (\boldsymbol{\omega}_{pro,i} \times \boldsymbol{\delta}_i) = 2\dot{q}_i \boldsymbol{\omega}_i \times \mathbf{e}_i + q_i \dot{\boldsymbol{\omega}}_i \times \mathbf{e}_i + q_i \boldsymbol{\omega}_i \times (\boldsymbol{\omega}_i \times \mathbf{e}_i) + \ddot{q}_i \mathbf{e}_i \tag{54}$$

The angular acceleration $\dot{\boldsymbol{\omega}}_i$ has no component along the axis of the ith intermediate shafts, and we have $\mathbf{e}_i \times (\dot{\boldsymbol{\omega}}_i \times \mathbf{e}_i) = \dot{\boldsymbol{\omega}}_i$. As a result, through cross multiplying both sides of Eq. (54) by $\mathbf{e}_i$, we can find $\dot{\boldsymbol{\omega}}_i$, as

$$\dot{\boldsymbol{\omega}}_i = (1/q_i)(\mathbf{e}_i \times (\dot{\boldsymbol{\omega}}_{pro,i} \times \boldsymbol{\delta}_i) + \mathbf{e}_i \times (\boldsymbol{\omega}_{pro,i} \times (\boldsymbol{\omega}_{pro,i} \times \boldsymbol{\delta}_i)) - 2\dot{q}_i \boldsymbol{\omega}_i - q_i \mathbf{e}_i \times (\boldsymbol{\omega}_i \times (\boldsymbol{\omega}_i \times \mathbf{e}_i))) \tag{55}$$

Dot multiplying both sides of Eq. (27) by $\mathbf{e}_i$ yields

$$\dot{q}_i = \boldsymbol{\delta}_i \times \mathbf{e}_i^T \mathbf{J}_{pro,i} \dot{\boldsymbol{\theta}} \tag{56}$$

Substituting $\boldsymbol{\omega}_i$, $\boldsymbol{\omega}_{pro,i}$, $\dot{\boldsymbol{\omega}}_{pro,i}$ and $\dot{q}_i$ from Eqs. (31), (20), (50) and (56) into Eq. (55), and doing a rearranging leads to $\dot{\boldsymbol{\omega}}_i$ in terms of $\dot{\boldsymbol{\theta}}$ and $\ddot{\boldsymbol{\theta}}$, as follows:

$$\dot{\boldsymbol{\omega}}_i = \mathbf{J}_{\dot{\omega}i,1} \ddot{\boldsymbol{\theta}} + \mathbf{J}_{\dot{\omega}i,2} \dot{\boldsymbol{\theta}} \tag{57}$$

where $\mathbf{J}_{\dot{\omega}i,1}$ and $\mathbf{J}_{\dot{\omega}i,2}$ are obtained in Appendix B. The total angular acceleration of the ith intermediate shafts is

$$\dot{\boldsymbol{\omega}}_{sh,i} = \dot{\boldsymbol{\omega}}_i + \ddot{\theta}_i \mathbf{e}_i \tag{58}$$

https://doi.org/10.1017/S026357472100062X Published online by Cambridge University Press

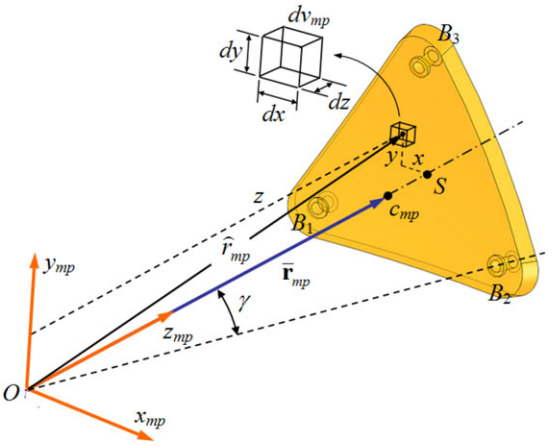

Figure 5. *A moving platform of the 3-PRR SPM and its differential volume dv_{mp}.*

After substituting $\dot{\boldsymbol{\omega}}_i$ from Eq. (57) into Eq. (58), and doing a rearranging, we get

$$\dot{\boldsymbol{\omega}}_{sh,i} = \mathbf{J}_{\dot{\omega},sh,i,1}\ddot{\boldsymbol{\theta}} + \mathbf{J}_{\dot{\omega},sh,i,2}\dot{\boldsymbol{\theta}} \tag{59}$$

where

$$\mathbf{J}_{\dot{\omega},sh,i,1} = \mathbf{J}_{\dot{\omega}i,1} + \begin{bmatrix} e_{ix}\mathbf{1}_{i\times(1-3)} \\ e_{iy}\mathbf{1}_{i\times(1-3)} \\ e_{iz}\mathbf{1}_{i\times(1-3)} \end{bmatrix} \tag{60a}$$

$$\mathbf{J}_{\dot{\omega},sh,i,2} = \mathbf{J}_{\dot{\omega}i,2} \tag{60b}$$

Consequently, we can obtain angular accelerations of the cylinder and piston of the ith driveshaft in terms of $\dot{\boldsymbol{\theta}}$ and $\ddot{\boldsymbol{\theta}}$, as

$$\dot{\boldsymbol{\omega}}_{cyl,i} = \mathbf{J}_{\dot{\omega},cyl,i,1}\ddot{\boldsymbol{\theta}} + \mathbf{J}_{\dot{\omega},cyl,i,2}\dot{\boldsymbol{\theta}} \tag{61a}$$

$$\dot{\boldsymbol{\omega}}_{pis,i} = \mathbf{J}_{\dot{\omega},pis,i,1}\ddot{\boldsymbol{\theta}} + \mathbf{J}_{\dot{\omega},pis,i,2}\dot{\boldsymbol{\theta}} \tag{61b}$$

where

$$\mathbf{J}_{\dot{\omega},cyl,i,1} = \mathbf{J}_{\dot{\omega},pis,i,1} = \mathbf{J}_{\dot{\omega},sh,i,1} \tag{62a}$$

$$\mathbf{J}_{\dot{\omega},cyl,i,2} = \mathbf{J}_{\dot{\omega},pis,i,2} = \mathbf{J}_{\dot{\omega},sh,i,2} \tag{62b}$$

6. Masses and inertia properties of the 3-PRR SPM

In the following sections, $\bar{\mathbf{I}}_a$, $a \in \{mp, pro, dis, cyl, pis\}$ is inertia matrix of the link a in the local coordinate frame attached to its mass center, and m_a is mass of link a.

6.1. Mass and inertia properties of the moving platform

The detailed explanations of the following formulations for m_{mp}, $\bar{\mathbf{r}}_{mp}$ and $\bar{\mathbf{I}}_{mp}$ are presented in Appendix C. Figure 5 shows the equilateral triangle-shaped moving platform of the manipulator. The mass of the moving platform is calculated using the following formula:

$$m_{mp} = \frac{3\sqrt{3}}{4}\rho_{mp}\,\hat{r}_{mp}^{2}\,t_{mp}\sin^2\gamma \tag{63}$$

https://doi.org/10.1017/S026357472100062X Published online by Cambridge University Press

where $\widehat{r}_{mp}$ is the radius of the moving platform spherical plate, t_{mp} is the thickness of the moving platform spherical plate, and ρ_{mp} is the density of the moving platform. The position vector of the mass center of the moving platform in O–$x_{mp}y_{mp}z_{mp}$ frame is given as

$$\bar{\mathbf{r}}_{mp} = [\,\bar{x}_{mp} \quad \bar{y}_{mp} \quad \bar{z}_{mp}\,]^T \tag{64}$$

where

$$\bar{x}_{mp} = \bar{y}_{mp} = 0 \tag{65a}$$

$$\bar{z}_{mp} = \frac{3\sqrt{3}}{4m_{mp}} \rho_{mp}\, \widehat{r}_{mp}^{\,3}\, t_{mp} \sin^2\gamma \tag{65b}$$

As well, the 3×3 inertia matrix $\bar{\mathbf{I}}_{mp}$ is

$$\bar{\mathbf{I}}_{mp} = \begin{bmatrix} I_{xx,mp} & I_{xy,mp} & I_{xz,mp} \\ I_{xy,mp} & I_{yy,mp} & I_{yz,mp} \\ I_{xz,mp} & I_{yz,mp} & I_{zz,mp} \end{bmatrix} \tag{66}$$

where

$$I_{xx,mp} = \frac{3\sqrt{3}}{32} \rho_{mp}\, \widehat{r}_{mp}^{\,4}\, t_{mp} \sin^4\gamma + \frac{3\sqrt{3}}{4} \rho_{mp}\, \widehat{r}_{mp}^{\,4}\, t_{mp} \sin^2\gamma + \frac{\sqrt{3}}{16} \rho_{mp}\, \widehat{r}_{mp}^{\,2}\, t_{mp}^3 \sin^2\gamma \tag{67a}$$

$$I_{yy,mp} = I_{xx,mp} \tag{67b}$$

$$I_{zz,mp} = \frac{3\sqrt{3}}{16} \rho_{mp}\, \widehat{r}_{mp}^{\,4}\, t_{mp} \sin^4\gamma \tag{67c}$$

$$I_{xy,mp} = \frac{3\sqrt{3}}{4} \rho_{mp}\, \widehat{r}_{mp}^{\,4}\, t_{mp} \sin^2\gamma + \frac{\sqrt{3}}{16} \rho_{mp}\, \widehat{r}_{mp}^{\,2}\, t_{mp}^3 \sin^2\gamma \tag{67d}$$

$$I_{xz,mp} = I_{yz,mp} = \frac{1}{2} I_{zz,mp} \tag{67e}$$

Subsequently, the inertia matrix of the moving platform in the base coordinate frame O-xyz is calculated as

$$\mathbf{I}_{mp} = \mathbf{R}_{mp} \bar{\mathbf{I}}_{mp} \mathbf{R}_{mp}^T \tag{68}$$

6.2. Mass and inertia matrix of the ith distal link

The detailed explanations of the following formulations for m_{dis}, $\bar{\mathbf{r}}_{dis}$ and $\bar{\mathbf{I}}_{dis}$ are presented in Appendix D. Figure 6 shows the distal link of the ith PRR leg of the manipulator as a curved solid bar with arc radius $\widehat{r}_{dis}$ and cross-section radius r_{cs}. The mass of the distal link is

$$m_{dis} = \pi \rho_{dis} r_{cs}^2\, \widehat{r}_{dis}\, \alpha \tag{69}$$

where ρ_{dis} is the density of the distal link. $\bar{\mathbf{r}}_{dis}$ will be

$$\bar{\mathbf{r}}_{dis} = [\,\bar{x}_{dis} \quad \bar{y}_{dis} \quad \bar{z}_{dis}\,]^T \tag{70}$$

https://doi.org/10.1017/S026357472100062X Published online by Cambridge University Press

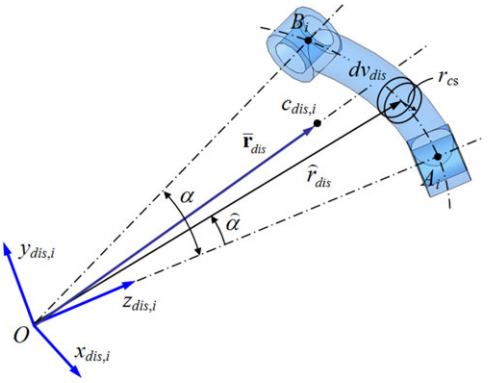

Figure 6. *The ith distal link of 3-PRR SPM and its volume differential* dv_{dis}.

where

$$\bar{x}_{dis} = 0 \tag{71a}$$

$$\bar{y}_{dis} = \frac{\pi \rho_{dis} r_{cs}^2 \hat{r}_{dis}^2 (1 - \cos\alpha)}{m_{dis}} \tag{71b}$$

$$\bar{z}_{dis} = \frac{\pi \rho_{dis} r_{cs}^2 \hat{r}_{dis}^2 \sin\alpha}{m_{dis}} \tag{71c}$$

The 3×3 inertia matrix $\bar{\mathbf{I}}_{dis}$ is given by

$$\bar{\mathbf{I}}_{dis} = \begin{bmatrix} I_{xx,dis} & I_{xy,dis} & I_{xz,dis} \\ I_{xy,dis} & I_{yy,dis} & I_{yz,dis} \\ I_{xz,dis} & I_{yz,dis} & I_{zz,dis} \end{bmatrix} \tag{72}$$

where

$$I_{xx,dis} = \pi \rho_{dis} r_{cs}^2 \hat{r}_{dis}^3 \alpha \tag{73a}$$

$$I_{yy,dis} = \pi \rho_{dis} r_{cs}^2 \hat{r}_{dis}^3 \left(\frac{\alpha}{2} + \frac{\sin 2\alpha}{4}\right) \tag{73b}$$

$$I_{zz,dis} = \pi \rho_{dis} r_{cs}^2 \hat{r}_{dis}^3 \left(\frac{\alpha}{2} - \frac{\sin 2\alpha}{4}\right) \tag{73c}$$

$$I_{xy,dis} = I_{yy,dis} \tag{73d}$$

$$I_{xz,dis} = I_{zz,dis} \tag{73e}$$

$$I_{yz,dis} = 0 \tag{73f}$$

Consequently, the inertia matrix of the *i*th distal link in the base coordinate frame *O-xyz* is calculated as

$$\mathbf{I}_{dis,i} = \mathbf{R}_{dis,i} \bar{\mathbf{I}}_{dis} \mathbf{R}_{dis,i}^T \tag{74}$$

6.3. Mass and inertia matrices of the other moving links

Other required quantities in dynamic analysis of the manipulator are masses m_{pro}, m_{cyl}, m_{pis}, mass center positions $\bar{\mathbf{r}}_{pro}$, l_{cyl} and l_{pis} and inertia matrices $\bar{\mathbf{I}}_{pro}$, $\bar{\mathbf{I}}_{cyl}$ and $\bar{\mathbf{I}}_{pis}$. These quantities are obtained from the CAD model of the corresponding link in SolidWorks software.

https://doi.org/10.1017/S026357472100062X Published online by Cambridge University Press

Table I. *The identified parameters of Stribeck's friction in the curved prismatic joints [32].*

F_c	F_s	F_v	v_s	ξ
0.1151	0.1759	0.66493	0.005	1.00

Inertia matrices of the proximal link and of the cylinder and piston of the ith driveshaft in the base coordinate frame O-xyz are calculated, respectively, as

$$\mathbf{I}_{pro,i} = \mathbf{R}_{pro,i}\bar{\mathbf{I}}_{pro}\mathbf{R}_{pro,i}^T \tag{75a}$$

and

$$\mathbf{I}_{cyl,i} = \mathbf{R}_{sh,i}\left[\bar{\mathbf{I}}_{cyl} + m_{cyl}l_{cyl}^2\left(\mathbf{e}_i^T\mathbf{e}_i\mathbf{1}_{3\times3} - \mathbf{e}_i\mathbf{e}_i^T\right)\right]\mathbf{R}_{sh,i}^T \tag{75b}$$

$$\mathbf{I}_{pis,i} = \mathbf{R}_{sh,i}\left[\bar{\mathbf{I}}_{pis} + m_{pis}(q_i - l_{pis})^2\left(\mathbf{e}_i^T\mathbf{e}_i\mathbf{1}_{3\times3} - \mathbf{e}_i\mathbf{e}_i^T\right)\right]\mathbf{R}_{sh,i}^T \tag{75c}$$

7. Dynamic equation of the 3-PRR SPM

In Section 9, values of internal moments between links are constrained to avoid large deflections of the links. To this aim, the Newton–Euler approach is adopted here to formulate the dynamic equation of the 3-PRR SPM, and the internal moments between links are computed necessarily. It is assumed that the gravitational forces are the only external forces acting on the proximal and distal links of the manipulator. The magnitude of frictional moment between the ith proximal link and its curved guide is computed using the Stribeck's formula [31, 32] as

$$\tau_{f,pro,i} = \left(F_c + (F_s - F_c)e^{-\left|\frac{r_{pro,i}\dot{\beta}_i}{v_s}\right|^{\xi}} + F_v r_{pro,i}\dot{\beta}_i\right) r_{pro,i} \tag{76}$$

where $r_{pro,i} = \left\|\mathbf{r}_{pro,i}\right\|$, and F_c, F_s and F_v are coefficients of Coulomb friction, static friction, viscous friction, respectively. Moreover, v_s is called Stribeck velocity and exponent ξ is a given constant. The values of these parameters are given in Table I.

Taking moments about the reference point O, Euler's equation for the intermediate shafts of the ith driveshaft will be

$$\begin{aligned}&\tau_{act,i}\mathbf{k} + \boldsymbol{\tau}_{dis,sh,i} + m_{cyl}\mathbf{r}_{cyl,i}\times\mathbf{g} + m_{pis}\mathbf{r}_{pis,i}\times\mathbf{g} - m_{cyl}\mathbf{r}_{cyl,i}\times\mathbf{a}_{cyl,i} - m_{pis}\mathbf{r}_{pis,i}\times\mathbf{a}_{pis,i}\\ &\quad -\mathbf{I}_{cyl,i}\dot{\boldsymbol{\omega}}_{cyl,i} - \mathbf{I}_{pis,i}\dot{\boldsymbol{\omega}}_{pis,i} - \boldsymbol{\omega}_{cyl,i}\times\mathbf{I}_{cyl,i}\boldsymbol{\omega}_{cyl,i} - \boldsymbol{\omega}_{pis,i}\times\mathbf{I}_{pis,i}\boldsymbol{\omega}_{pis,i} = \mathbf{0}\end{aligned} \tag{77a}$$

Let $\tau_{f,i,1}$ and $\tau_{f,i,2}$ be magnitudes of frictional moments of the revolute joints at A_i and B_i, respectively. Euler's equations for the proximal and distal links of the ith PRR leg are, respectively, as

$$\boldsymbol{\tau}_{dis,pro,i} - \tau_{f,pro,i}\mathbf{n}_i + \tau_{f,i,1}\mathbf{u}_i + m_{pro}\mathbf{r}_{pro,i}\times\mathbf{g} - m_{pro}\mathbf{r}_{pro,i}\times\mathbf{a}_{pro,i} - \mathbf{I}_{pro,i}\dot{\boldsymbol{\omega}}_{pro,i} - \boldsymbol{\omega}_{pro,i}\times\mathbf{I}_{pro,i}\boldsymbol{\omega}_{pro,i} = \mathbf{0} \tag{77b}$$

$$\begin{aligned}&\boldsymbol{\tau}_{mp,dis,i} - \boldsymbol{\tau}_{dis,sh,i} - \boldsymbol{\tau}_{dis,pro,i} - \tau_{f,i,1}\mathbf{u}_i + \tau_{f,i,2}\mathbf{v}_i + m_{dis}\mathbf{r}_{dis,i}\times\mathbf{g} - m_{dis}\mathbf{r}_{dis,i}\times\mathbf{a}_{dis,i}\\ &\quad -\mathbf{I}_{dis,i}\dot{\boldsymbol{\omega}}_{dis,i} - \boldsymbol{\omega}_{dis,i}\times\mathbf{I}_{dis,i}\boldsymbol{\omega}_{dis,i} = \mathbf{0}\end{aligned} \tag{77c}$$

where $\mathbf{g} = [0\ 0\ -9.81]^T$ is the vector of gravitational acceleration, and $\boldsymbol{\tau}_{a,b,i}$, $a, b \in \{mp, pro, dis, sh\}$ is the internal moment that link a of the ith leg acts on its link b. Taking moments about point O, Euler's equation for the moving platform becomes

$$\boldsymbol{\tau}_{ext} + m_{mp}\mathbf{r}_{mp}\times\mathbf{g} - \sum_{i=1}^{3}\boldsymbol{\tau}_{mp,dis,i} - \sum_{i=1}^{3}\tau_{f,i,2}\mathbf{v}_i - m_{mp}\mathbf{r}_{mp}\times\mathbf{a}_{mp} - \mathbf{I}_{mp}\dot{\boldsymbol{\omega}}_{mp} - \boldsymbol{\omega}_{mp}\times\mathbf{I}_{mp}\boldsymbol{\omega}_{mp} = \mathbf{0} \tag{78}$$

https://doi.org/10.1017/S026357472100062X Published online by Cambridge University Press

where $\boldsymbol{\tau}_{ext}$ is the external moment acting on the moving platform. We obtain $\boldsymbol{\tau}_{mp,dis,i}$ from Eq. (77c) and introduce it into Eq. (78), as follows:

$$\boldsymbol{\tau}_{ext} + m_{mp}\mathbf{r}_{mp} \times \mathbf{g} - m_{mp}\mathbf{r}_{mp} \times \mathbf{a}_{mp} - \mathbf{I}_{mp}\dot{\boldsymbol{\omega}}_{mp} - \boldsymbol{\omega}_{mp} \times \mathbf{I}_{mp}\boldsymbol{\omega}_{mp} - \sum_{i=1}^{3} \boldsymbol{\tau}_{dis,pro,i} - \sum_{i=1}^{3} \boldsymbol{\tau}_{dis,sh,i}$$
$$- \sum_{i=1}^{3} \tau_{f,i,1}\mathbf{u}_i + \sum_{i=1}^{3} (m_{dis}\mathbf{r}_{dis,i} \times \mathbf{g} - m_{dis}\mathbf{r}_{dis,i} \times \mathbf{a}_{dis,i} - \mathbf{I}_{dis,i}\dot{\boldsymbol{\omega}}_{dis,i} - \boldsymbol{\omega}_{dis,i} \times \mathbf{I}_{dis,i}\boldsymbol{\omega}_{dis,i}) = \mathbf{0} \tag{79}$$

Then, we obtain $\boldsymbol{\tau}_{dis,sh,i}$ and $\boldsymbol{\tau}_{dis,pro,i}$ from Eqs. (77a) and (77b), and introduce them into Eq. (79) which yields

$$\sum_{i=1}^{3} \tau_{act,i}\mathbf{k} + \boldsymbol{\tau}_{ext} - \sum_{i=1}^{3} \tau_{f,pro,i}\mathbf{n}_i + m_{mp}\mathbf{r}_{mp} \times \mathbf{g} - m_{mp}\mathbf{r}_{mp} \times \mathbf{a}_{mp} - \mathbf{I}_{mp}\dot{\boldsymbol{\omega}}_{mp} - \boldsymbol{\omega}_{mp} \times \mathbf{I}_{mp}\boldsymbol{\omega}_{mp}$$
$$+ \sum_{i=1}^{3} (m_{cyl}\mathbf{r}_{cyl,i} \times \mathbf{g} + m_{pis}\mathbf{r}_{pis,i} \times \mathbf{g} + m_{pro}\mathbf{r}_{pro,i} \times \mathbf{g} + m_{dis}\mathbf{r}_{dis,i} \times \mathbf{g})$$
$$- \sum_{i=1}^{3} (m_{cyl}\mathbf{r}_{cyl,i} \times \mathbf{a}_{cyl,i} + m_{pis}\mathbf{r}_{pis,i} \times \mathbf{a}_{pis,i} + m_{pro}\mathbf{r}_{pro,i} \times \mathbf{a}_{pro,i} + m_{dis}\mathbf{r}_{dis,i} \times \mathbf{a}_{dis,i}) \tag{80}$$
$$- \sum_{i=1}^{3} (\mathbf{I}_{cyl,i}\dot{\boldsymbol{\omega}}_{cyl,i} + \mathbf{I}_{pis,i}\dot{\boldsymbol{\omega}}_{pis,i} + \mathbf{I}_{pro,i}\dot{\boldsymbol{\omega}}_{pro,i} + \mathbf{I}_{dis,i}\dot{\boldsymbol{\omega}}_{dis,i})$$
$$- \sum_{i=1}^{3} (\boldsymbol{\omega}_{cyl,i} \times \mathbf{I}_{cyl,i}\boldsymbol{\omega}_{cyl,i} + \boldsymbol{\omega}_{pis,i} \times \mathbf{I}_{pis,i}\boldsymbol{\omega}_{pis,i} + \boldsymbol{\omega}_{pro,i} \times \mathbf{I}_{pro,i}\boldsymbol{\omega}_{pro,i} + \boldsymbol{\omega}_{dis,i} \times \mathbf{I}_{dis,i}\boldsymbol{\omega}_{dis,i}) = \mathbf{0}$$

Where the acceleration of mass centers of the manipulator's moving links are given by

$$\mathbf{a}_{\kappa} = \dot{\boldsymbol{\omega}}_{\kappa} \times \mathbf{r}_{\kappa} + \boldsymbol{\omega}_{\kappa} \times (\boldsymbol{\omega}_{\kappa} \times \mathbf{r}_{\kappa}) \tag{81}$$

while subscript $\kappa \in \{$"*mp*", "*cyl*,*i*", "*pis*,*i*", "*pro*,*i*", "*dis*,*i*"$\}$. Finally, substituting $\boldsymbol{\omega}_{mp}$, $\boldsymbol{\omega}_{pro,i}$, $\boldsymbol{\omega}_{dis,i}$, $\boldsymbol{\omega}_{cyl.i}$, $\boldsymbol{\omega}_{pis,i}$, $\dot{\boldsymbol{\omega}}_{mp}$, $\dot{\boldsymbol{\omega}}_{pro,i}$, $\dot{\boldsymbol{\omega}}_{dis,i}$, $\dot{\boldsymbol{\omega}}_{cyl.i}$, $\dot{\boldsymbol{\omega}}_{pis,i}$ and $\mathbf{a}_{\kappa}$ from Eqs. (15), (20), (23), (36), (45), (50), (52), (61) and (81) into Eq. (80) and doing a rearranging leads to the closed-form dynamic equation of the 3-PRR SPM in terms of $\dot{\boldsymbol{\theta}}$ and $\ddot{\boldsymbol{\theta}}$, as follows:

$$\mathbf{I}(\boldsymbol{\theta})\ddot{\boldsymbol{\theta}} + \mathbf{C}(\boldsymbol{\theta}, \dot{\boldsymbol{\theta}})\dot{\boldsymbol{\theta}} + \mathbf{T}(\boldsymbol{\theta}) + \boldsymbol{\tau}_{act} = \mathbf{0} \tag{82}$$

where $\boldsymbol{\tau}_{act} = [\tau_{act,1}\ \tau_{act,2}\ \tau_{act,3}]^T$ is the vector of actuator torques. Moreover,

$$\mathbf{I}(\boldsymbol{\theta}) = \mathbf{K}^{-1}\left(\mathbf{I}_{mp}\mathbf{J}_{\dot{\omega},mp,1} + \sum_{i=1}^{3}\left(\mathbf{I}_{pro,i}\mathbf{J}_{\dot{\omega},pro,i,1} + \mathbf{I}_{dis,i}\mathbf{J}_{\dot{\omega},dis,i,1} - \mathbf{I}_{cyl,i}\mathbf{J}_{\dot{\omega},cyl,i,1} + \mathbf{I}_{pis,i}\mathbf{J}_{\dot{\omega},pis,i,1}\right) + \mathbf{G}_1\right) \tag{83a}$$

$$\mathbf{C}(\boldsymbol{\theta}, \dot{\boldsymbol{\theta}}) = \mathbf{K}^{-1}\left(\mathbf{I}_{mp}\mathbf{J}_{\dot{\omega},mp,2} + \sum_{i=1}^{3}\left(\mathbf{I}_{pro,i}\mathbf{J}_{\dot{\omega},pro,i,2} + \mathbf{I}_{dis,i}\mathbf{J}_{\dot{\omega},dis,i,2} - \mathbf{I}_{cyl,i}\mathbf{J}_{\dot{\omega},cyl,i,2} + \mathbf{I}_{pis,i}\mathbf{J}_{\dot{\omega},pis,i,2}\right) + \mathbf{G}_2\right) \tag{83b}$$

$$\mathbf{T}(\boldsymbol{\theta}) = \mathbf{K}^{-1}\begin{pmatrix}\boldsymbol{\tau}_{ext} - \sum_{i=1}^{3} \tau_{f,pro,i}\mathbf{n}_i + m_{mp}\mathbf{r}_{mp} \times \mathbf{g} \\ + \sum_{i=1}^{3}\left(m_{pro}\mathbf{r}_{pro,i} \times \mathbf{g} + m_{dis}\mathbf{r}_{dis,i} \times \mathbf{g} + m_{cyl}\mathbf{r}_{cyl,i} \times \mathbf{g} + m_{pis}\mathbf{r}_{pis,i} \times \mathbf{g}\right)\end{pmatrix} \tag{83c}$$

https://doi.org/10.1017/S026357472100062X Published online by Cambridge University Press

with 3×3 matrices $\mathbf{G}_1$ and $\mathbf{G}_2$ given in Appendix E, and

$$\mathbf{K} = \begin{bmatrix} 0 & 0 & 0 \\ 0 & 0 & 0 \\ 1 & 1 & 1 \end{bmatrix} \tag{84}$$

$\mathbf{I}(\boldsymbol{\theta})$ and $\mathbf{C}(\boldsymbol{\theta}, \dot{\boldsymbol{\theta}})$ are 3×3 the inertia and Coriolis matrices of the manipulator, and $\mathbf{T}(\boldsymbol{\theta})$ is the 3×1 vector of the external moment and the gravitational forces.

8. Dynamic dexterity of the 3-PRR SPM

Dynamic dexterity of a high-speed manipulator can be interpreted as the ability of changing acceleration (or deceleration) by actuator forces/torques [33]. Conventionally, the condition number of the inertia matrix of the dynamic equation is proposed to evaluate the dynamic dexterity of manipulators when the difference between the easiest direction and the hardest direction is the main issue [34]. For the 3-PRR SPM, the condition number of the inertia matrix is defined as

$$1 \leq \kappa_I = \frac{\sigma_{\mathrm{I,max}}}{\sigma_{\mathrm{I,min}}} \leq \infty \tag{85}$$

where $\sigma_{\mathbf{I},max}$ and $\sigma_{\mathbf{I},min}$ are the maximum and minimum singular values of the inertia matrix $\mathbf{I}(\theta)$ at a given configuration of the manipulator. In order to bound $\kappa_{\mathbf{I}}$, one may consider its inverse value, that is $1/\kappa_{\mathbf{I}}$, which is defined as *dynamic conditioning index* (DCI) and ranges between 0 and 1. Particularly, in a pose where DCI is equal to 1, the manipulator has a dynamic isotropy, indicating that the acceleration of the moving platform is insensitive to variation of actuator torques. In contrast, if DCI is equal to 0, small changes of actuator torques lead to a big change of the acceleration of the moving platform. In other words, the less the DCI is the more shock the moving platform experience during the motion of the manipulator.

DCI of the 3-PRR SPM is plotted in Fig. 7 for three sets of α, γ and φ_z showing that the manipulator has a larger dynamic dexterity near the central region of the workspace than at its boundaries. Thus, DCI should also be considered in the design process of the manipulator, so that the moving platform avoids the workspace boundaries as much as possible.

9. Torque minimization of the 3-PRR SPM

In order to reduce actuator loads, the magnitude of the maximum torque experienced by the manipulator actuators should be minimized. To this aim, a constrained optimization problem is presented to find an optimal design of the manipulator for a given repetitive task, while the values of actuator torques are minimal. The above formulations are programmed in Matlab software. Moreover, to verify the mathematical results, dynamics of the manipulator are also simulated using the SimMechanics toolbox of Matlab software.

The following relations define the orientation of the moving platform as the function of time

$$\begin{aligned} \varphi_x(t) &= \pi/8 \text{ rad} \\ \varphi_y(t) &= 0 \text{ rad} \\ \varphi_z(t) &= t \text{ rad} \end{aligned} \tag{86}$$

where $0 \leq t \leq 2\pi$ s. If it is assumed that the moving platform moves on a surface of a sphere with a radius of unity ($\widehat{r}_{mp} = 1$ m), then with relations (86), point S of the moving platform moves on a circle centered at point C' (0, 0, 0.924) with radius 0.383 m (Fig. 8), and returns to its initial location after 2π s.

https://doi.org/10.1017/S026357472100062X Published online by Cambridge University Press

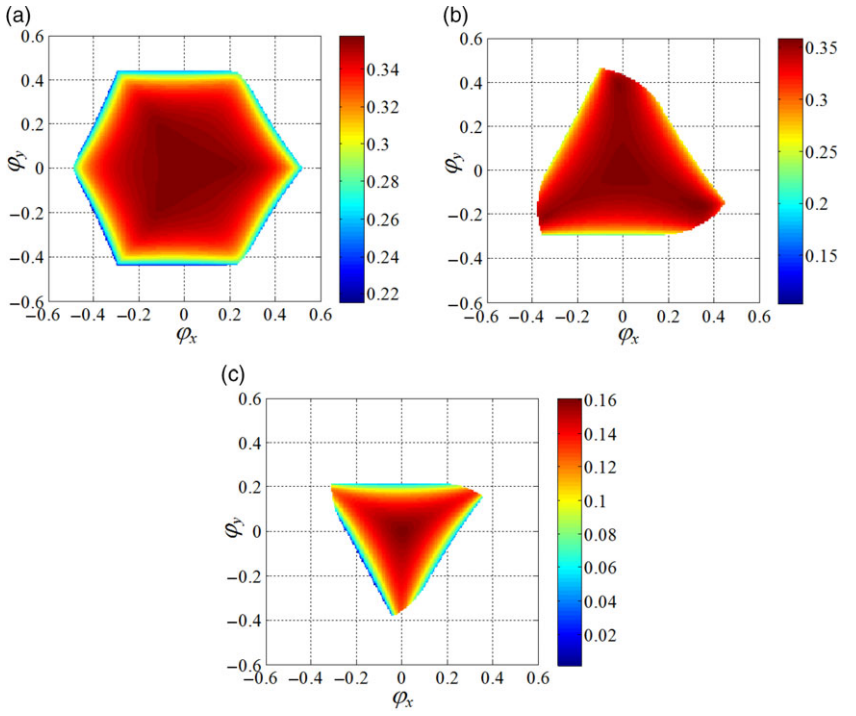

Figure 7. *DCI of the 3-PRR SPM for (a) $\alpha = 25°$, $\gamma = 8.5°$, $\varphi_z = 0°$, (b) $\alpha = 22°$, $\gamma = 10°$, $\varphi_z = 30°$, (c) $\alpha = 17°$, $\gamma = 12°$, $\varphi_z = -40°$.*

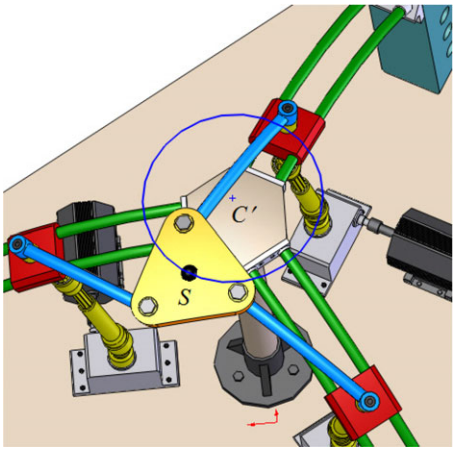

Figure 8. *The given circular trace of point S of the moving platform.*

The objective function to be minimized is defined as

$$f(\mathbf{x}) = \frac{\sum_{i=1}^{3} \left(\tau_{act,i,\min}^2 + \tau_{act,i,\max}^2\right)}{6\tau_{all}^2} \tag{87}$$

where $\tau_{act,i,\min}$ ($\tau_{act,i,\max}$) is the minimum (maximum) value of $\tau_{act,i}$ along the circular path, and τ_{all} is the maximum allowable value of actuator torques. Here we take τ_{all} = 100 N.m. Note that $0 \leq f(\mathbf{x}) \leq 1$, and the closer the value of $f(\mathbf{x})$ is to zero, the smaller the values of actuator torques are along the

https://doi.org/10.1017/S026357472100062X Published online by Cambridge University Press

circular path. The actuator torques $\tau_{act,i,\min}$ and $\tau_{act,i,\max}$ depend on values of parameters m_{mp}, $\bar{\mathbf{I}}_{mp}$, m_{dis} and $\bar{\mathbf{I}}_{dis}$, and also on the positions of gearboxes, that is, d and h (Fig. 4). As represented in Eqs. (63), (66), (69) and (72), the first four parameters depend on γ and α, and h is a known dimension of the gearboxes. Thus, for the optimization problem, we take $\mathbf{x} = [\gamma, \alpha, d]^T$ as the vector of design variables. These design parameters should be between their minimum and maximum allowable values:

$$\mathrm{ct}_1: \gamma_{\min} \leq \gamma \leq \gamma_{\max} \tag{88a}$$

$$\mathrm{ct}_2: \alpha_{\min} \leq \alpha \leq \alpha_{\max} \tag{88b}$$

$$\mathrm{ct}_3: d_{\min} \leq d \leq d_{\max} \tag{88c}$$

The following kinematic constraints [1] should also be considered during the design of the manipulator. The inverse position kinematics should have a real solution for each leg of the manipulator; this leads to

$$\mathrm{ct}_4: (\tilde{A}_i^2 - \tilde{C}_i^2 + \tilde{B}_i^2) \geq 0 \tag{89}$$

where [1]

$$\begin{aligned} \tilde{A}_i &= \sin\psi_1 {}^m\mathbf{v}_i^T \mathbf{R}_{mp,1\times(1-3)} - \cos\psi_1 {}^m\mathbf{v}_i^T \mathbf{R}_{mp,2\times(1-3)} \\ \tilde{B}_i &= {}^m\mathbf{v}_i^T \mathbf{R}_{mp,3\times(1-3)} \\ \tilde{C}_i &= \cos\alpha \end{aligned} \tag{90}$$

with $\mathbf{R}_{mp,i\times(1-3)}$ denoting the ith row of matrix $\mathbf{R}_{mp}$ in Eq. (2), and ${}^m\mathbf{v}_i$ representing vector $\mathbf{v}_i$ in the local frame O–$x_{mp}y_{mp}z_{mp}$, such that

$${}^m\mathbf{v}_i = [\cos\psi_i \sin\gamma \quad \sin\psi_i \sin\gamma \quad \cos\gamma\,]^T \tag{91}$$

For each point in the workspace, the stroke of the ith curved prismatic joint should be between 0 and its maximum allowable value, β_{max}:

$$\mathrm{ct}_5: 0 \leq \beta_i \leq \beta_{\max} \tag{92}$$

To eliminate any void in the workspace of each P$\underline{\text{R}}$R leg of the manipulator, the following constraint equation is imposed:

$$\mathrm{ct}_6: \alpha < \frac{\beta_{\max}}{2} \tag{93}$$

To avoid leg interferences between distal links, the below conditions are also considered for i = 1, 2, 3:

$$\mathrm{ct}_7: \alpha'_i > \alpha \text{ or } \alpha'_{i+1} > \alpha \text{ modulo } 3 \tag{94}$$

where $\alpha'_i = \angle(\mathbf{u}_i, \mathbf{p}_i)$ and $\alpha'_{i+1} = \angle(\mathbf{u}_i, \mathbf{p}_{i+1})$ and $\mathbf{p}_i$ is a unit vector along the intersection line of the planes passing through distal links A_iB_i and $A_{i+1}B_{i+1}$ modulo 3 (Fig. 9). The method to compute α'_i and α'_{i+1} are presented in Appendix F.

The smaller angle between axes of the driving and driven shafts of a Rzeppa joint should be less than its maximum allowable value, λ_{max}. For two Rzeppa joints of the ith actuating system at D_i and E_i (Fig. 10), this condition is written respectively as

$$\mathrm{ct}_8: \lambda_{Di} < \lambda_{\max} \tag{95a}$$

$$\mathrm{ct}_9: \lambda_{Ei} < \lambda_{\max} \tag{95b}$$

where $\lambda_{Di} = \angle(\mathbf{k}, \mathbf{e}_i)$ and $\lambda_{Ei} = \angle(\mathbf{u}_i, \mathbf{e}_i)$. It is assumed that the kinematic conditioning index (KCI) and DCI satisfy minimum values during the motion of the manipulator, such that

$$\mathrm{ct}_{10}: \mathrm{KCI} \geq kci_{\min} \tag{96a}$$

$$\mathrm{ct}_{11}: \mathrm{DCI} \geq dci_{\min} \tag{96b}$$

https://doi.org/10.1017/S026357472100062X Published online by Cambridge University Press

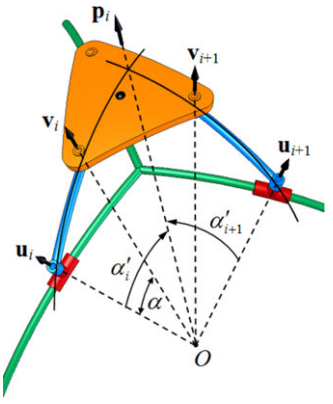

Figure 9. *The intersection line of the planes passing through distal links A_iB_i and $A_{i+1}B_{i+1}$ modulo 3 [1].*

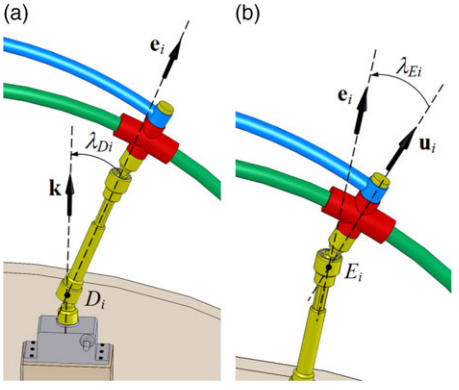

Figure 10. *Axis angles of the ith double Rzeppa-type driveshaft: (a) lower Rzeppa joint at D_i and (b) upper Rzeppa joint at E_i [1].*

KCI is the ratio of the smallest to the largest singular values of the Jacobian matrix $\mathbf{J}_{mp}$ at a configuration of the manipulator [1]. The larger the kci_{min} is, the farther the point S is from singularities [1]. Moreover, the larger the dci_{min} is, the nearer the point S will be to the central region of the manipulator workspace.

To avoid large deflections in intermediate shafts of the driveshafts and distal links, the moments inserted on these links are constrained respectively as follows:

$$\mathrm{ct}_{12}\colon (\tau_{act,i}\mathbf{k} + \boldsymbol{\tau}_{dis,sh,i})^T \mathbf{e}_i \leq 100 \text{ N.m} \tag{97a}$$

$$\mathrm{ct}_{13}\colon (\boldsymbol{\tau}_{mp,dis,i} - \boldsymbol{\tau}_{dis,sh,i})^T \mathbf{i}_{dis,i} \leq 100 \text{ N.m} \tag{97b}$$

$$\mathrm{ct}_{14}\colon (\boldsymbol{\tau}_{mp,dis,i} - \boldsymbol{\tau}_{dis,sh,i})^T \mathbf{k}_{dis,i} \leq 100 \text{ N.m} \tag{97c}$$

where the moments $\boldsymbol{\tau}_{dis,sh,i}$ and $\boldsymbol{\tau}_{mp,sh,i}$ are calculated from Eqs. (77) easily. In addition, the actuator torques should be less than τ_{all} along the circular path, namely

$$\mathrm{ct}_{15}\colon \tau_{act,i} < \tau_{\mathrm{all}} \tag{98}$$

Using the objective function in Eq. (87) and design constraints (88)–(98), the constrained optimization problem of 3-P<u>R</u>R PPM is formulated as follows:

$$\text{Minimize } f(\mathbf{x}) \tag{99}$$

$$\text{subject to } \mathrm{ct}_j, j = 1, 2, 3, \ldots, 15 \tag{100}$$

https://doi.org/10.1017/S026357472100062X Published online by Cambridge University Press

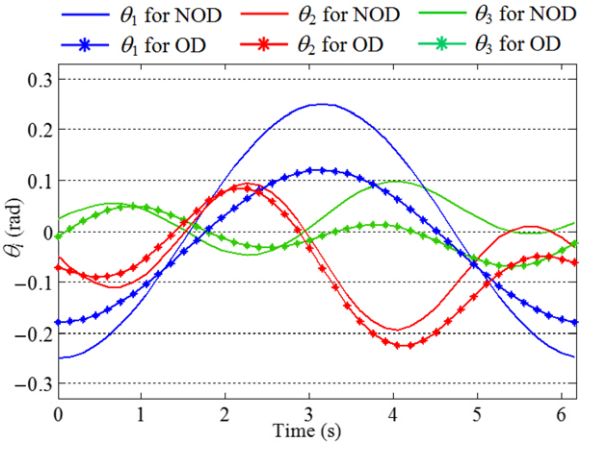

Figure 11. *Rotation angles of actuated revolute joints for non-optimal (NOD) and optimal (OD) designs.*

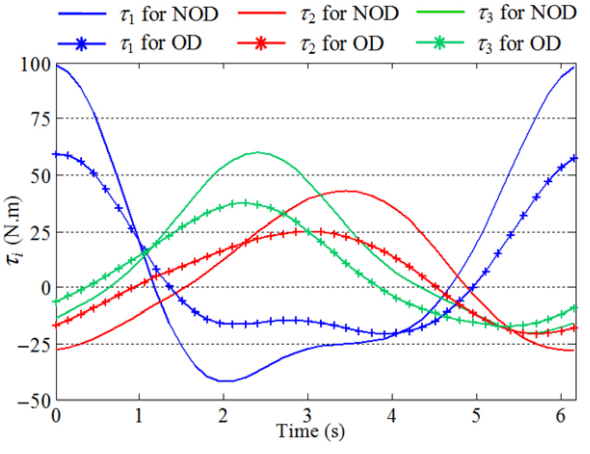

Figure 12. *Torques of actuators for non-optimal (NOD) and optimal (OD) designs.*

The moving platform and distal links are made up of aluminum alloy with uniform densities $\rho_{mp} = \rho_{dis} = 2810$ kg/m^3. Other geometrical and mass properties of the manipulator are given in Appendix G.

In the first step, we solve inverse dynamics of the manipulator with architectural parameters: $\gamma = 8.5°$, $\alpha = 25°$, $d = 0.5$ m. It is assumed that no external moment acts on the moving platform ($\boldsymbol{\tau}_{ext} = \mathbf{0}$). To calculate the actuator torques, Eq. (82) is rewritten as

$$\boldsymbol{\tau}_{act} = -\mathbf{I}(\boldsymbol{\theta})\ddot{\boldsymbol{\theta}} - \mathbf{C}(\boldsymbol{\theta}, \dot{\boldsymbol{\theta}})\dot{\boldsymbol{\theta}} - \mathbf{T}(\boldsymbol{\theta}) \tag{101}$$

Rotation angles of actuators θ_i for this non-optimal design (NOD) are computed as functions of time using the inverse position kinematic analysis [1], as presented in Fig. 11; then velocity and acceleration vectors $\dot{\boldsymbol{\theta}}$ and $\ddot{\boldsymbol{\theta}}$ are computed using Eqs. (15) and (45) as

$$\dot{\boldsymbol{\theta}} = \mathbf{J}_{mp}^{-1}\boldsymbol{\omega}_{mp} \tag{102}$$

$$\ddot{\boldsymbol{\theta}} = \mathbf{J}_{\dot{\omega},mp,1}^{-1}\dot{\boldsymbol{\omega}}_{mp} - \mathbf{J}_{\dot{\omega},mp,1}^{-1}\mathbf{J}_{\dot{\omega},mp,2}\dot{\boldsymbol{\theta}} \tag{103}$$

Now, we can compute all terms on the right-hand side of Eq. (101), which leads to time history of $\boldsymbol{\tau}_{act}$, as shown in Fig. 12.

In the second step, we consider the optimization problem with $\gamma_{min} = 10°$, $\gamma_{max} = 30°$, $\alpha_{min} = 10°$, $\alpha_{max} = 45°$, $d_{min} = 0.35$ m, $d_{max} = 0.60$ m, $\beta_{max} = 60°$ and $\lambda_{max} = 45°$. Values of other geometrical and

https://doi.org/10.1017/S026357472100062X Published online by Cambridge University Press

Table II. *Values of $\tau_{i,\min}$ (N.m), $\tau_{i,\max}$(N.m) and $f(\boldsymbol{x})$ (N^2.m^2) for non-optimal and optimal designs of 3-PRR PPM.*

Design type	$\tau_{act,1,min}$	$\tau_{act,1,max}$	$\tau_{act,2,min}$	$\tau_{act,2,max}$	$\tau_{act,3,min}$	$\tau_{act,3,max}$	$f(\boldsymbol{x})$
Non-optimal design	−41.85	97.76	−28.17	42.97	−20.24	60.23	0.30
Optimal design	−20.47	59.26	−20.51	24.92	−17.13	37.43	0.12

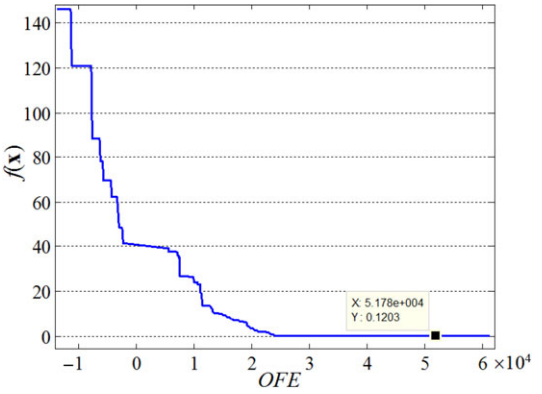

Figure 13. *Convergence graph of the optimization process for the best result.*

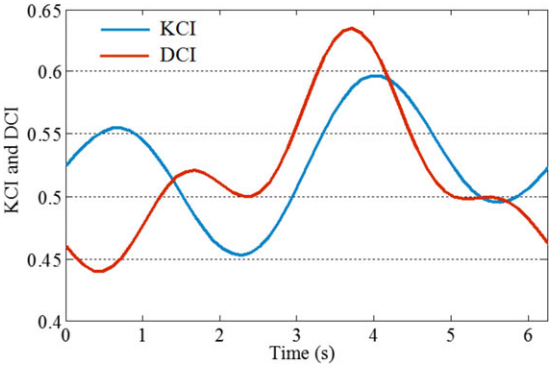

Figure 14. *KCI and DCI of the optimal design of 3-PRR SPM along the circular path.*

mass properties are the same as the ones used in previous step. The PSO algorithm [35] is applied here to minimize the objective function $f(\mathbf{x})$. The optimization problem is solved for different values of kci_{min} and $dci_{min} \in \{0.3, 0.35, 0.4, 0.45, 0.5, 0.55\}$. The best result of 15 independent runs is $f(\mathbf{x}) = 0.16$ for $kci_{min} = 0.45$ and $dci_{min} = 0.4$. The corresponding values of design parameters are $\gamma = 12.02°$, $\alpha = 21.69°$, $d = 0.54$ m. Convergence graph of the optimization process is shown in Fig. 13 revealing that the GEO algorithm yields the best result after 5.178×10^4 objective function evaluations (*OFE*). Time histories of rotation angles and actuator torques for this optimal design (OD) are also represented in Figs. 11 and 12. As well, the resultant values of $\tau_{act,i,\min}$, $\tau_{act,i,\max}$ and $f(\mathbf{x})$ for both optimal and non-optimal designs are also listed in Table II. Comparing these values, one can see that the values of $\tau_{act,i,\min}$, $\tau_{act,i,\max}$ and $f(\mathbf{x})$ have decreased significantly after optimization. KCI and DCI are plotted in Fig. 14 for the optimal design revealing that KCI ≥ 0.45 and DCI ≥ 0.4 along the circular path.

https://doi.org/10.1017/S026357472100062X Published online by Cambridge University Press

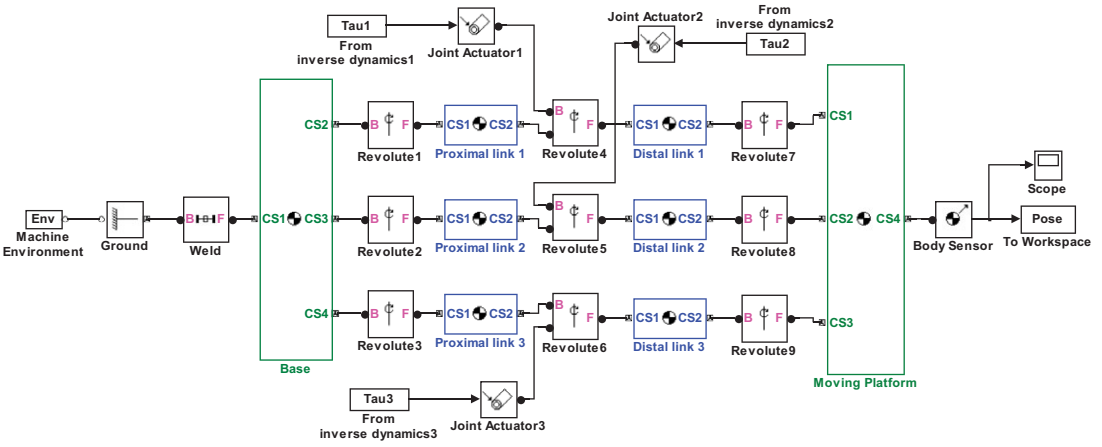

Figure 15. *SimMechanics model for forward dynamics of the 3-PRR SPM.*

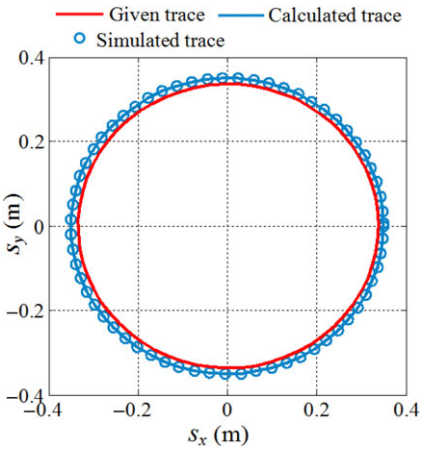

Figure 16. *The given, calculated and simulated traces of point S of the moving platform.*

To further verify the results, outputs of the inverse dynamic analysis (i.e., the calculated actuator torques in Fig. 12) of the optimal design are applied as the input for the forward dynamic analysis. To this aim, we rewrite Eq. (82) as

$$\ddot{\boldsymbol{\theta}} = -\mathbf{I}^{-1}(\boldsymbol{\theta})(\boldsymbol{\tau}_{act} + \mathbf{C}(\boldsymbol{\theta}, \dot{\boldsymbol{\theta}})\dot{\boldsymbol{\theta}} + \mathbf{T}(\boldsymbol{\theta})) \tag{104}$$

Initial conditions of actuators (at $t = 0$) are obtained using the inverse position kinematic analysis [1] and Eq. (102), as follows:

$$\theta_1(0) = -0.18 \text{ rad}, \theta_2(0) = -0.07 \text{ rad}, \theta_3(0) = -0.01 \text{ rad}$$

$$\dot{\theta}_1(0) = 0.23 \text{ rad/s}^2, \dot{\theta}_2(0) = 0.81 \text{ rad/s}^2, \dot{\theta}_3(0) = -0.09 \text{ rad/s}^2$$

The SimMechanics model for the forward dynamic analysis is presented in Fig. 15. With the above-calculated actuator torques and initial conditions, the terms on the right-hand side of Eq. (103) and consequently $\ddot{\boldsymbol{\theta}}$ is calculated. Then, we can compute new values of $\dot{\boldsymbol{\theta}}$ and $\boldsymbol{\theta}$ through the integration of $\ddot{\boldsymbol{\theta}}$. With the obtained value of $\boldsymbol{\theta}$, the unique and acceptable pose of the moving platform is identified using the method presented in ref. [1]. This process is repeated to obtain orientations ($\varphi_x(t)$, $\varphi_y(t)$, $\varphi_z(t)$) of

https://doi.org/10.1017/S026357472100062X Published online by Cambridge University Press

the moving platform during motion. As a consequence, the trace of point S of the moving platform can be obtained by the following relation:

$$s(t) = [\,\mathbf{R}_{mp,13}(t) \quad \mathbf{R}_{mp,23}(t) \quad \mathbf{R}_{mp,33}(t)\,]^T \tag{105}$$

where $\mathbf{R}_{mp,i3}(t)$ for $i = 1, 2, 3$ denotes the third column of matrix $\mathbf{R}_{mp}$. The given and calculated traces of point S along with the trace obtained by the SimMechanics model are plotted in Fig. 16. Investigating the results in Fig. 16 reveals that the calculated trace of point S by the forward dynamic analysis is coincident with the trace obtained by the SimMechanics model. This verifies correctness and efficiency of the presented dynamic modeling of the star-shaped base 3-P$\underline{\text{R}}$R SPM. However, there is a slight difference of 0.012 m between a radius of those two traces and of the given trace. This variation is due to the simplifications which were made in calculating inertia matrices of the moving platform and distal links.

10. Conclusion

This paper addressed dynamic analysis and torque minimization of a novel symmetrical 3-P$\underline{\text{R}}$R SPM. After description of the manipulator structure, the local coordinate frames and rotation matrices were established for its moving links. Complete velocity and acceleration analyses were performed to obtain velocity and acceleration of the manipulator moving links in terms of $\dot{\boldsymbol{\theta}}$ and $\ddot{\boldsymbol{\theta}}$. The dynamic equation of the 3-P$\underline{\text{R}}$R SPM was formulated in a closed form using the Newton–Euler method. It was shown that the Newton–Euler approach is an efficient method to find values of internal moments between links of the manipulator. A constrained optimization problem was also presented to minimize actuator torques, while the moving platform of the manipulator moves along a given circular path. Many kinematic and dynamic constraints including KCI, DCI and internal moments between links were considered. The closeness of given trace of point S of the moving platform to the trace obtained by mathematical and SimMechanics models verified correctness and efficiency of the proposed dynamic modeling. The author hopes that the present study provides a robust framework for future research in areas of control and motion planning of the proposed 3-P$\underline{\text{R}}$R SPM.

Funding. This research is not funded by a specific project grant.

Conflict of Interest. The author declares that he has no conflict of interest.

References

[1] S. Zarkandi, "Kinematic analysis and optimal design of a novel 3-P$\underline{\text{R}}$R spherical parallel manipulator," *Proc. Inst. Mech. Eng. Part C J. Mech. Eng. Sci.* (2020). https://doi.org/10.1177%2F0954406220938806.

[2] S. Park, J. Kim and G. Lee "Optimal trajectory planning considering optimal torque distribution of redundantly actuated parallel mechanism," *Proc. Inst. Mech. Eng. Part C J. Mech. Eng. Sci.* **232**(23), 4410–4419 (2018). doi:10.1177/0954406217751818.

[3] S. Baressi Šegota, N. Anđelić, I. Lorencin, M. Saga and Z. Car, "Path planning optimization of six-degree-of-freedom robotic manipulators using evolutionary algorithms," *Int. J. Adv. Rob. Syst.* (2020). doi:10.1177/1729881420908076.

[4] A. K. Gillawat and H. J. Nagarsheth Human Upper Limb Joint Torque Minimization Using Genetic Algorithm. **In:** *Recent Advances in Mechanical Engineering*, *Lecture Notes in Mechanical Engineering* (H. Kumar and P. Jain, eds.) (Springer, Singapore, 2020). https://doi.org/10.1007/978-981-15-1071-7_6.

[5] H. Saafi, M. A. Laribi and S. Zeghloul, "Optimal torque distribution for a redundant 3-RRR spherical parallel manipulator used as a haptic medical device," *Rob. Auto. Syst.* **89**, 40–50 (2017). https://doi.org/10.1016/j.robot.2016.12.005.

[6] J. Yao, W. Gu, Z. Feng, L. Chen, Y. Xu and Y. Zhao, "Dynamic analysis and driving force optimization of a 5-DOF parallel manipulator with redundant actuation," *Rob. Comput. Integr. Manuf.* **48**, 51–58 (2017). https://doi.org/10.1016/j.rcim.2017.02.006.

[7] R. Boudreau, J. Léger, H. Tinaou and A. Gallant, "Dynamic analysis and optimization of a kinematically redundant planar parallel manipulator," *Trans. Canad. Soc. Mech. Eng*. **42**(1), 20–29 (2018). https://doi.org/10.1139/tcsme-2017-0003.

[8] C. M. Gosselin and J. Wang, "Singularity loci of a special class of spherical three-degree-of-freedom parallel mechanisms with revolute actuators," *Int. J. Rob. Res*. **21**(7), 649–659 (2002). doi:10.1177/027836402322023231.
[9] S. Staicu, "Recursive modeling in dynamics of Agile wrist spherical parallel robot," *Rob. Comput. Integr. Manuf.* **25**(2), 409–416 (2009). https://doi.org/10.1016/j.rcim.2008.02.001.
[10] S. Staicu, "Dynamics of the spherical 3-UPS/S parallel mechanism with prismatic actuators," *Multibody Syst. Dyn*. **22**, 115–132 (2009). https://doi.org/10.1007/s11044-009-9150-x.
[11] J. Enferadi and A. Akbarzadeh Tootoonchi, "Inverse dynamics analysis of a general spherical star-triangle parallel manipulator using principle of virtual work," *Nonlinear Dyn.* **61**(3), 419–434 (2010).
[12] A. Akbarzadeh and J. Enferadi, "A virtual work based algorithm for solving direct dynamics problem of a 3-RRP spherical parallel manipulator," *J. Intell. Rob. Syst.* **63**, 25–49 (2011). https://doi.org/10.1007/s10846-010-9469-9.
[13] T. Sun, Y. Song, G. Dong, B. Lian and J. Liu, "Optimal design of a parallel mechanism with three rotational degrees of freedom," *Rob. Comput. Integr. Manuf.* **28**(4), 500–508 (2012). https://doi.org/10.1016/j.rcim.2012.02.002.
[14] L. J. Puglisi, R. J. Saltaren, G. R. Portoles, H. Moreno, P. F. Cardenas and C. Garcia, "Design and kinematic analysis of 3PSS-1S wrist for needle insertion guidance," Rob. Auto. Syst. 61(5), 417–427 (2013).
[15] G. Wu, S. Caro, Sh. Bai and J. Kepler, "Dynamic modeling and design optimization of a 3-DOF spherical parallel manipulator," *Rob. Auto. Syst.* **62**(10), 1377–1386 (2014).
[16] Y. Zhaon, K. Qiu, Sh. Wang and Z. Zhang, "Inverse kinematics and rigid-body dynamics for a three rotational degrees of freedom parallel manipulator," *Rob. Comput. Integr. Manuf.* **31**, 40–50 (2015). https://doi.org/10.1016/j.rcim.2014.07.002.
[17] H. Khoshnoodi, A. Rahmani Hanzaki and H. A. Talebi, Kinematics, "Singularity study and optimization of an innovative spherical parallel manipulator with large workspace," *J. Intell. Rob. Syst.* **92**, 309–321 (2018). https://doi.org/10.1007/s10846-017-0752-x.
[18] G. Wu and Sh. Bai, "Design and kinematic analysis of a 3-RRR spherical parallel manipulator reconfigured with four–bar linkages," *Rob. Comput. Integr. Manuf.* **56**, 55–65 (2019). https://doi.org/10.1016/j.rcim.2018.08.006.
[19] J. Enferadi and K. Jafari, "A Kane's based algorithm for closed-form dynamic analysis of a new design of a 3RSS-S spherical parallel manipulator," *Multibody Syst. Dyn.* **49**, 377–394 (2020). https://doi.org/10.1007/s11044-020-09736-y.
[20] H. Saafi, M. Amine Laribi and S. Zeghloul, "Forward kinematic model improvement of a spherical parallel manipulator using an extra sensor," *Mech. Mach. Theory* **91**, 102–119 (2015). https://doi.org/10.1016/j.mechmachtheory.2015.04.006.
[21] S. Zarkandi, "Kinematic and dynamic modeling of a planar parallel manipulator served as CNC tool holder," *Int. J. Dyn. Control* **6**(1), 14–28 (2018).
[22] S. Pedrammehr, B. Danaei, H. Abdi, M. T. Masouleh and S. Nahavandi, "Dynamic analysis of Hexarot: Axis-symmetric parallel manipulator," *Robotica* **36**(2), 225–240 (2018). doi:10.1017/S0263574717000315.
[23] S. Zarkandi, "Inverse and forward dynamics of a 4RSS+PS parallel manipulator with one infinite rotational motion," *Aust. J. Mech. Eng.* (2020). doi:10.1080/14484846.2020.1714352.
[24] O. Altuzarra, A. Zubizarreta, I. Cabanes and C. Pinto, "Dynamics of a four degrees-of-freedom parallel manipulator with parallelogram joints," *Mechatronics* **19**(8), 1269–1279 (2009). https://doi.org/10.1016/j.mechatronics.2009.08.003.
[25] M.-J. Liu, C.-X. Li and C.-N. Li, "Dyamics analysis of the Gough–Stewart Platform manipulator," *IEEE Trans. Rob. Autom.* **16**(1), 94–98 (2000).
[26] J. Gallardo, J. M. Rico and A. Frisoli, "Dynamics of parallel manipulators by means of screw theory," *Mech. Mach. Theory* **38**(11), 1113–1131 (2003).
[27] A. Akbarzadeh, J. Enferadi and M. Sharifnia, "Dynamics analysis of a 3-RRP spherical parallel manipulator using the natural orthogonal complement," *Multibody Sys. Dyn.* **29**(4), 361–380 (2013).
[28] K. Sugimoto, "Kinematics and dynamic analysis of parallel manipulator by means of motor algebra," *ASME J. Mech., Trans. Autom. Des.* **109**(1), 3–7 (1987).
[29] S. Zarkandi, "A new geometric method for singularity analysis of spherical mechanisms," *Robotica* **29**(7), 1083–1092 (2011). https://doi.org/10.1017/S0263574711000385.
[30] Euler angles, Wikipedia, The Free Encyclopedia, https://en.wikipedia.org/w/index.php?title=Euler_angles&oldid=996258926 (accessed January 23, 2021).
[31] R. Stribeck, "The key qualities of sliding and roller bearings," *Zeitschrift des Vereines Seutscher Ingenieure* **46**(38), 39 (1902).
[32] X. Tu, Y. F. Zhou, P. Zhao and X. Cheng, "Modeling the static friction in a robot joint by genetically optimized BP neural network," *J. Intell. Rob. Syst.* **94**, 29–41 (2019), https://doi.org/10.1007/s10846-018-0796-6.
[33] T. Yoshikawa, "Dynamic Manipulability of Robot Manipulators," *IEEE International Conference on Robotics and Automation (ICRA)*, vol. 2 (1985) pp. 1033–1038.
[34] J. Wu, J. Wang, T. Li, L. Wang and L. Guan, "Dynamic dexterity of a planar 2-DOF parallel manipulator in a hybrid machine tool," *Robotica* **26**(1), 93–98 (2008). doi:10.1017/S0263574707003621.
[35] X. Hu, R. C. Eberhart and Y. Shi, "Engineering optimization with particle swarm," *Proceedings of the 2003 IEEE Swarm Intelligence Symposium*, Indianapolis, USA (2003) pp. 53–57. doi:10.1109/SIS.2003.1202247.

Appendix A

Considering $\dot{\beta}_i$, $\dot{\eta}_i$, $\boldsymbol{\omega}_{mp}$ and $\dot{\boldsymbol{\omega}}_{mp}$ in Eqs. (18), (41), (15) and (45), the terms at the right-hand side of Eq. (48) become
The first term:

$$\frac{(\mathbf{u}_i \times \mathbf{v}_i)^T (\mathbf{J}_{\dot{\omega},mp,1}\ddot{\boldsymbol{\theta}} + \mathbf{J}_{\dot{\boldsymbol{\omega}},mp,2}\dot{\boldsymbol{\theta}})}{(\mathbf{u}_i \times \mathbf{v}_i)^T \mathbf{n}_i}\mathbf{n}_i = \mathbf{J}_{\dot{\omega},pro,i,1}\ddot{\boldsymbol{\theta}} + \mathbf{J}^1_{\dot{\omega},pro,i,2}\dot{\boldsymbol{\theta}} \tag{A1}$$

where

$$\mathbf{J}_{\dot{\omega},pro,i,1} = \frac{1}{(\mathbf{u}_i \times \mathbf{v}_i)^T \mathbf{n}_i}\begin{bmatrix} n_{ix}(\mathbf{u}_i \times \mathbf{v}_i)^T \mathbf{J}_{\dot{\omega},mp,1} \\ n_{iy}(\mathbf{u}_i \times \mathbf{v}_i)^T \mathbf{J}_{\dot{\omega},mp,1} \\ n_{iz}(\mathbf{u}_i \times \mathbf{v}_i)^T \mathbf{J}_{\dot{\omega},mp,1} \end{bmatrix} \tag{A2}$$

$$\mathbf{J}^1_{\dot{\omega},pro,i,2} = (1/(\mathbf{u}_i \times \mathbf{v}_i)^T \mathbf{n}_i)\begin{bmatrix} n_{ix}(\mathbf{u}_i \times \mathbf{v}_i)^T \mathbf{J}_{\dot{\omega},mp,2} \\ n_{iy}(\mathbf{u}_i \times \mathbf{v}_i)^T \mathbf{J}_{\dot{\omega},mp,2} \\ n_{iz}(\mathbf{u}_i \times \mathbf{v}_i)^T \mathbf{J}_{\dot{\omega},mp,2} \end{bmatrix} \tag{A3}$$

The second term:

$$-\frac{(\mathbf{u}_i \times \mathbf{v}_i)^T (\mathbf{n}_i \times \mathbf{u}_i)}{(\mathbf{u}_i \times \mathbf{v}_i)^T \mathbf{n}_i}\left(\frac{(\mathbf{u}_i \times \mathbf{v}_i)^T \mathbf{J}_{mp}\dot{\boldsymbol{\theta}}}{\mathbf{n}_i^T(\mathbf{u}_i \times \mathbf{v}_i)}\right)\mathbf{1}_{i\times(1-3)}\dot{\boldsymbol{\theta}}\mathbf{n}_i = \mathbf{J}^2_{\dot{\omega},pro,i,2}\dot{\boldsymbol{\theta}} \tag{A4}$$

where

$$\mathbf{J}^2_{\dot{\omega},pro,i,2} = -\frac{(\mathbf{u}_i \times \mathbf{v}_i)^T (\mathbf{n}_i \times \mathbf{u}_i)}{(\mathbf{u}_i \times \mathbf{v}_i)^T \mathbf{n}_i}\left(\frac{(\mathbf{u}_i \times \mathbf{v}_i)^T \mathbf{J}_{mp}\dot{\boldsymbol{\theta}}}{\mathbf{n}_i^T(\mathbf{u}_i \times \mathbf{v}_i)}\right)\begin{bmatrix} n_{ix}\mathbf{1}_{i\times(1-3)} \\ n_{iy}\mathbf{1}_{i\times(1-3)} \\ n_{iz}\mathbf{1}_{i\times(1-3)} \end{bmatrix} \tag{A5}$$

The third term:

$$-\frac{1}{(\mathbf{u}_i \times \mathbf{v}_i)^T \mathbf{n}_i}\left(\frac{(\mathbf{n}_i \times \mathbf{u}_i)^T \mathbf{J}_{mp}\dot{\boldsymbol{\theta}}}{(\mathbf{n}_i \times \mathbf{u}_i)^T \mathbf{v}_i}\right)\mathbf{1}_{\mathbf{i}\times(1-3)}\dot{\boldsymbol{\theta}}\mathbf{n}_i = \mathbf{J}^3_{\dot{\boldsymbol{\omega}},pro,i,2}\dot{\boldsymbol{\theta}} \tag{A6}$$

where

$$\mathbf{J}^3_{\dot{\omega},pro,i,2} = -\frac{1}{(\mathbf{u}_i \times \mathbf{v}_i)^T \mathbf{n}_i}\left(\frac{(\mathbf{n}_i \times \mathbf{u}_i)^T \mathbf{J}_{mp}\dot{\boldsymbol{\theta}}}{(\mathbf{n}_i \times \mathbf{u}_i)^T \mathbf{v}_i}\right)\begin{bmatrix} n_{ix}\mathbf{1}_{i\times(1-3)} \\ n_{iy}\mathbf{1}_{i\times(1-3)} \\ n_{iz}\mathbf{1}_{i\times(1-3)} \end{bmatrix} \tag{A7}$$

Note that

$$\mathbf{J}_{\dot{\omega},pro,i,1} = \mathbf{J}_{pro,i} \tag{A8}$$

where $\mathbf{J}_{pro,i}$ was defined before in Eq. (21), and $\mathbf{J}_{\dot{\omega},pro,i,2}$ is computed as follows:

$$\mathbf{J}_{\dot{\omega},pro,i,2} = \sum_{k=1}^{3}\mathbf{J}^k_{\dot{\omega},pro,i,2} \tag{A9}$$

Appendix B

Considering relation (29), Eq. (55) is rewritten as

$$\dot{\boldsymbol{\omega}}_i = (1/q_i)\left(\left(\mathbf{e}_i^T\boldsymbol{\delta}_i\right)\dot{\boldsymbol{\omega}}_{pro,i} - \left(\mathbf{e}_i^T\dot{\boldsymbol{\omega}}_{pro,i}\right)\boldsymbol{\delta}_i\right) + \left(\mathbf{e}_i^T\left(\boldsymbol{\omega}_{pro,i} \times \boldsymbol{\delta}_i\right)\right)\boldsymbol{\omega}_{pro,i} - \left(\mathbf{e}_i^T\boldsymbol{\omega}_{pro,i}\right)\boldsymbol{\omega}_{pro,i} \times \boldsymbol{\delta}_i$$
$$-2\dot{q}_i\boldsymbol{\omega}_i + q_i\left(\mathbf{e}_i^T\boldsymbol{\omega}_i\right)\boldsymbol{\omega}_i \times \mathbf{e}_i\big) \tag{B1}$$

Now, substituting $\boldsymbol{\omega}_{pro,i}$, $\dot{\boldsymbol{\omega}}_{pro,i}$, $\boldsymbol{\omega}_i$ and $\dot{q}_i$ from Eqs. (20), (50), (31) and (56) into Eq. (B1), the terms at the right-hand side of this latter equation are summarized as follows: The first term:

$$(1/q_i)(\mathbf{e}_i^T\boldsymbol{\delta}_i)\dot{\boldsymbol{\omega}}_{pro,i} = (1/q_i)(\mathbf{e}_i^T\boldsymbol{\delta}_i)(\mathbf{J}_{\dot{\boldsymbol{\omega}},pro,i,1}\ddot{\boldsymbol{\theta}} + \mathbf{J}_{\dot{\boldsymbol{\omega}},pro,i,2}\dot{\boldsymbol{\theta}}) = \mathbf{J}^1_{\dot{\boldsymbol{\omega}}i,1}\ddot{\boldsymbol{\theta}} + \mathbf{J}^1_{\dot{\boldsymbol{\omega}}i,2}\dot{\boldsymbol{\theta}} \tag{B2}$$

where

$$\mathbf{J}^1_{\dot{\boldsymbol{\omega}}i,1} = (1/q_i)(\mathbf{e}_i^T\boldsymbol{\delta}_i)\mathbf{J}_{\dot{\boldsymbol{\omega}},pro,i,1} \tag{B3}$$

$$\mathbf{J}^1_{\dot{\boldsymbol{\omega}}i,2} = (1/q_i)(\mathbf{e}_i^T\boldsymbol{\delta}_i)\mathbf{J}_{\dot{\boldsymbol{\omega}},pro,i,2} \tag{B4}$$

https://doi.org/10.1017/S026357472100062X Published online by Cambridge University Press

The second term:

$$-(1/q_i)(\mathbf{e}_i^T\dot{\boldsymbol{\omega}}_{pro,i})\boldsymbol{\delta}_i = -(1/q_i)\mathbf{e}_i^T(\mathbf{J}_{\dot{\omega},pro,i,1}\ddot{\boldsymbol{\theta}} + \mathbf{J}_{\dot{\omega},pro,i,2}\dot{\boldsymbol{\theta}})\boldsymbol{\delta}_i = \mathbf{J}^2_{\dot{\omega}i,1}\ddot{\boldsymbol{\theta}} + \mathbf{J}^2_{\dot{\omega}i,2}\dot{\boldsymbol{\theta}} \tag{B5}$$

where

$$\mathbf{J}^2_{\dot{\omega}i,1} = -(1/q_i)\begin{bmatrix} \delta_{ix}\mathbf{e}_i^T\mathbf{J}_{\dot{\omega},pro,i,1} \\ \delta_{iy}\mathbf{e}_i^T\mathbf{J}_{\dot{\omega},pro,i,1} \\ \delta_{iz}\mathbf{e}_i^T\mathbf{J}_{\dot{\omega},pro,i,1} \end{bmatrix} \tag{B6}$$

$$\mathbf{J}^2_{\dot{\omega}i,2} = -(1/q_i)\begin{bmatrix} \delta_{ix}\mathbf{e}_i^T\mathbf{J}_{\dot{\omega},pro,i,2} \\ \delta_{iy}\mathbf{e}_i^T\mathbf{J}_{\dot{\omega},pro,i,2} \\ \delta_{iz}\mathbf{e}_i^T\mathbf{J}_{\dot{\omega},pro,i,2} \end{bmatrix} \tag{B7}$$

The third term:

$$(1/q_i)(\mathbf{e}_i^T(\boldsymbol{\omega}_{pro,i}\times\boldsymbol{\delta}_i))\boldsymbol{\omega}_{pro,i} = (1/q_i)(\mathbf{e}_i^T(\mathbf{J}_{pro,i}\dot{\boldsymbol{\theta}}\times\boldsymbol{\delta}_i))\mathbf{J}_{pro,i}\dot{\boldsymbol{\theta}} = \mathbf{J}^3_{\dot{\omega}i,2}\dot{\boldsymbol{\theta}} \tag{B8}$$

where

$$\mathbf{J}^3_{\dot{\omega}i,2} = (1/q_i)(\mathbf{e}_i^T(\mathbf{J}_{pro,i}\dot{\boldsymbol{\theta}}\times\boldsymbol{\delta}_i))\mathbf{J}_{pro,i} \tag{B9}$$

The fourth term:

$$-(1/q_i)(\mathbf{e}_i^T\boldsymbol{\omega}_{pro,i})\boldsymbol{\omega}_{pro,i}\times\boldsymbol{\delta}_i = -(1/q_i)(\mathbf{e}_i^T\mathbf{J}_{pro,i}\dot{\boldsymbol{\theta}})\mathbf{J}_{pro,i}\dot{\boldsymbol{\theta}}\times\boldsymbol{\delta}_i = \mathbf{J}^4_{\dot{\omega}i,2}\dot{\boldsymbol{\theta}} \tag{B10}$$

where

$$\mathbf{J}^4_{\dot{\omega}i,2} = -(1/q_i)\begin{bmatrix} (\mathbf{e}_i^T\mathbf{J}_{pro,i}\dot{\boldsymbol{\theta}})(\mathbf{J}_{pro,i,2\times(1-3)}\delta_{iz} - \mathbf{J}_{pro,i,3\times(1-3)}\delta_{iy}) \\ (\mathbf{e}_i^T\mathbf{J}_{pro,i}\dot{\boldsymbol{\theta}})(\mathbf{J}_{pro,i,3\times(1-3)}\delta_{ix} - \mathbf{J}_{pro,i,1\times(1-3)}\delta_{iz}) \\ (\mathbf{e}_i^T\mathbf{J}_{pro,i}\dot{\boldsymbol{\theta}})(\mathbf{J}_{pro,i,1\times(1-3)}\delta_{iy} - \mathbf{J}_{pro,i,2\times(1-3)}\delta_{ix}) \end{bmatrix} \tag{B11}$$

The fifth term:

$$-(2/q_i)\dot{q}_i\boldsymbol{\omega}_i = -(2/q_i)((\boldsymbol{\delta}_i\times\mathbf{e}_i)^T\mathbf{J}_{pro,i}\dot{\boldsymbol{\theta}})\mathbf{J}_{\omega i}\dot{\boldsymbol{\theta}} = \mathbf{J}^5_{\dot{\omega}i,2}\dot{\boldsymbol{\theta}} \tag{B12}$$

where

$$\mathbf{J}^5_{\dot{\boldsymbol{\omega}}i,2} = -(2/q_i)((\boldsymbol{\delta}_i\times\mathbf{e}_i)^T\mathbf{J}_{pro,i}\dot{\boldsymbol{\theta}})\mathbf{J}_{\boldsymbol{\omega}i} \tag{B13}$$

The sixth term:

$$(\mathbf{e}_i^T\boldsymbol{\omega}_i)\boldsymbol{\omega}_i\times\mathbf{e}_i = (\mathbf{e}_i^T\mathbf{J}_{\omega i}\dot{\boldsymbol{\theta}})\mathbf{J}_{\omega i}\dot{\boldsymbol{\theta}}\times\mathbf{e}_i = \mathbf{J}^6_{\dot{\omega}i,2}\dot{\boldsymbol{\theta}} \tag{B14}$$

where

$$\mathbf{J}^6_{\dot{\omega}i,2} = \begin{bmatrix} (\mathbf{e}_i^T\mathbf{J}_{\omega i}\dot{\boldsymbol{\theta}})(\mathbf{J}_{\omega i,2\times(1-3)}e_{iz} - \mathbf{J}_{\omega i,3\times(1-3)}e_{iy}) \\ (\mathbf{e}_i^T\mathbf{J}_{\omega i}\dot{\boldsymbol{\theta}})(\mathbf{J}_{\omega i,3\times(1-3)}e_{ix} - \mathbf{J}_{\omega i,1\times(1-3)}e_{iz}) \\ (\mathbf{e}_i^T\mathbf{J}_{\omega i}\dot{\boldsymbol{\theta}})(\mathbf{J}_{\omega i,1\times(1-3)}e_{iy} - \mathbf{J}_{\omega i,2\times(1-3)}e_{ix}) \end{bmatrix} \tag{B15}$$

Finally, $\mathbf{J}_{\dot{\omega}i,1}$ and $\mathbf{J}_{\dot{\omega}i,2}$ are computed by the following relations:

$$\mathbf{J}_{\dot{\omega}i,1} = \mathbf{J}^1_{\dot{\omega}i,1} + \mathbf{J}^2_{\dot{\omega}i,1} \tag{B16}$$

$$\mathbf{J}_{\dot{\omega}i,2} = \sum_{k=1}^{6}\mathbf{J}^k_{\dot{\omega}i,2} \tag{B17}$$

Appendix C

Figure C.1 shows the projection of the moving platform on the *xy* plane.

Regarding Figs. 5 and C.1, equations of the lines, constituting boundaries of the moving platform projection on the *xy* plane, are:

$$y_1 = -(\widehat{r}_{mp}\sin\gamma)/2 \tag{C1}$$

$$y_2 = \sqrt{3}x + \widehat{r}_{mp}\sin\gamma \tag{C2}$$

$$y_3 = -\sqrt{3}x + \widehat{r}_{mp}\sin\gamma \tag{C3}$$

https://doi.org/10.1017/S026357472100062X Published online by Cambridge University Press

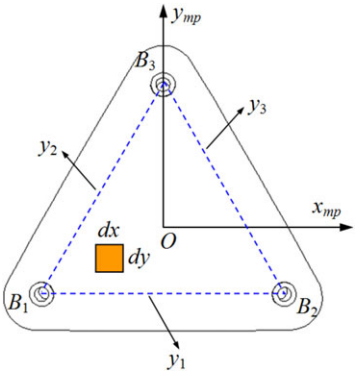

Figure C.1. *Projection of the moving platform on xy plane.*

Using these boundary equations, the mass of the moving platform in Eq. (63) is calculated through the following triple integral:

$$m_{mp} = \iiint \rho_{mp} dv_{mp} = \rho_{mp} \int_{\widehat{r}_{mp}-t_{mp}/2}^{\widehat{r}_{mp}+t_{mp}/2} \int_{-(\widehat{r}_{mp}\sin\gamma)/2}^{\widehat{r}_{mp}\sin\gamma} \int_{\sqrt{3}(y-\widehat{r}_{mp}\sin\gamma)/3}^{-\sqrt{3}(y-\widehat{r}_{mp}\sin\gamma)/3} dxdydz$$

$$= \frac{3\sqrt{3}}{4} \rho_{mp} \widehat{r}_{mp}^{2} t_{mp} \sin^2\gamma \tag{C4}$$

where differential $dv_{mp} = dxdydz$ denotes an infinitesimal volume of the moving platform. Then, components of the position vector $\bar{\mathbf{r}}_{mp}$ in Eq. (65) are obtained via the following integrals:

$$\bar{x}_{mp} = \frac{1}{m_{mp}} \iiint x \rho_{mp} dv_{mp} = 0 \tag{C5}$$

$$\bar{y}_{mp} = \frac{1}{m_{mp}} \iiint y \rho_{mp} dv_{mp} = 0 \tag{C6}$$

$$\bar{z}_{mp} = \frac{1}{m_{mp}} \iiint z \rho_{mp} dv_{mp} = \frac{3\sqrt{3}}{4m_{mp}} \rho_{mp} \widehat{r}_{mp}^{3} t_{mp} \sin^2\gamma \tag{C7}$$

The first array of an inertial matrix $\bar{\mathbf{I}}_{mp}$ in Eq. (67a) is calculated by the following triple integral:

$$I_{xx,mp} = \iiint (y^2 + z^2) \rho dv_{mp} = \rho_{mp} \int_{\widehat{r}_{mp}-t_{mp}/2}^{\widehat{r}_{mp}+t_{mp}/2} \int_{-(\widehat{r}_{mp}\sin\gamma)/2}^{\widehat{r}_{mp}\sin\gamma} \int_{\sqrt{3}(y-\widehat{r}_{mp}\sin\gamma)/3}^{-\sqrt{3}(y-\widehat{r}_{mp}\sin\gamma)/3} (y^2 + z^2) dxdydz$$

$$= \frac{3\sqrt{3}}{32} \rho_{mp} \widehat{r}_{mp}^{4} \sin\gamma^4 t_{mp} + \frac{3\sqrt{3}}{4} \rho_{mp} \widehat{r}_{mp}^{4} \sin\gamma^2 t_{mp} + \frac{\sqrt{3}}{16} \rho_{mp} \widehat{r}_{mp}^{2} \sin\gamma^2 t_{mp}^3 \tag{C8}$$

Other arrays of the matrix $\bar{\mathbf{I}}_{mp}$ are computed in a similar manner using the following triple integrals:

$$I_{yy,mp} = \iiint (x^2 + z^2) \rho dv_{mp} \tag{C9}$$

$$I_{zz,mp} = \iiint (x^2 + y^2) \rho dv_{mp} \tag{C10}$$

$$I_{xy,mp} = \iiint z^2 \rho dv_{mp} \tag{C11}$$

$$I_{xz,mp} = \iiint y^2 \rho dv_{mp} \tag{C12}$$

$$I_{yz,mp} = \iiint x^2 \rho dv_{mp} \tag{C13}$$

https://doi.org/10.1017/S026357472100062X Published online by Cambridge University Press

Appendix D

According to Fig. 6, the volume of each differential of the curved solid bar of the ith distal link is obtained as

$$dv_{dis} = \pi r_{cs}^2 \, \widehat{r}_{dis} \, d\,\widehat{\alpha} \tag{D1}$$

Therefore, the mass of the distal link in Eq. (69) can be calculated using the following triple integral:

$$m_{dis} = \iiint \rho_{dis} dv_{dis} = \rho_{dis} \int_0^{\alpha} \pi r_{cs}^2 \, \widehat{r}_{dis} \, d\,\widehat{\alpha} = \pi \rho_{dis} r_{cs}^2 \, \widehat{r}_{dis} \, \alpha \tag{D2}$$

Similarly, components of the vector $\bar{\mathbf{r}}_{dis}$ in Eq. (71) are calculated as

$$\bar{x}_{dis} = \frac{1}{m_{dis}} \iiint y \rho_{dis} dv_{dis} = 0 \tag{D3}$$

$$\bar{y}_{dis} = \frac{1}{m_{dis}} \iiint y \rho_{dis} dv_{dis} = \frac{\rho_{dis}}{m_{dis}} \int_0^{\alpha} (\widehat{r}_{dis} \sin\widehat{\alpha}) \pi r_{cs}^2 \, \widehat{r}_{dis} \, d\,\widehat{\alpha} = \frac{\pi \rho_{dis} r_{cs}^2 \, \widehat{r}_{dis}^{\,2} (1 - \cos\alpha)}{m_{dis}} \tag{D4}$$

$$\bar{z}_{dis} = \frac{1}{m_{dis}} \iiint z \rho_{dis} dv_{dis} = \frac{\rho_{dis}}{m_{dis}} \int_0^{\alpha} (\widehat{r}_{dis} \cos\widehat{\alpha}) \pi r_{cs}^2 \, \widehat{r}_{dis} \, d\,\widehat{\alpha} = \frac{\pi \rho_{dis} r_{cs}^2 \, \widehat{r}_{dis}^{\,2} \sin\alpha}{m_{dis}} \tag{D5}$$

Moreover, arrays of inertia matrix $\bar{\mathbf{I}}_{dis}$ in Eq. (73) are computed as follows:

$$I_{xx,dis} = \iiint (y^2 + z^2) \rho_{dis} dv_{dis} = \pi \rho_{dis} r_{cs}^2 \, \widehat{r}_{dis} \int_0^{\alpha} (\widehat{r}_{dis}^{\,2} \sin^2\widehat{\alpha} + \widehat{r}_{dis}^{\,2} \cos^2\widehat{\alpha}) d\,\widehat{\alpha} = \pi \rho_{dis} r_{cs}^2 \, \widehat{r}_{dis}^{\,3} \, \alpha \tag{D6}$$

$$I_{yy,dis} = \iiint (x^2 + z^2) \rho_{dis} dv_{dis} = \pi \rho_{dis} r_{cs}^2 \, \widehat{r}_{dis} \int_0^{\alpha} \widehat{r}_{dis}^{\,2} \cos^2\widehat{\alpha} \, d\,\widehat{\alpha} = \pi \rho_{dis} r_{cs}^2 \, \widehat{r}_{dis}^{\,3} \left(\frac{\alpha}{2} + \frac{\sin 2\alpha}{4} \right) \tag{D7}$$

$$I_{zz,dis} = \iiint (x^2 + y^2) \rho_{dis} dv_{dis} = \pi \rho_{dis} r_{cs}^2 \, \widehat{r}_{dis} \int_0^{\alpha} (\widehat{r}_{dis}^{\,2} \sin^2\widehat{\alpha}) d\,\widehat{\alpha} = \pi \rho_{dis} r_{cs}^2 \, \widehat{r}_{dis}^{\,3} \left(\frac{\alpha}{2} - \frac{\sin 2\alpha}{4} \right) \tag{D8}$$

$$I_{xy,dis} = \iiint z^2 \rho_{dis} dv_{dis} = I_{yy,dis} \tag{D9}$$

$$I_{xz,dis} = \iiint y^2 \rho_{dis} dv_{dis} = I_{zz,dis} \tag{D10}$$

$$I_{yz,dis} = \iiint x^2 \rho_{dis} dv_{dis} = 0 \tag{D11}$$

Appendix E

With $\mathbf{a}_{mp}$ in Eq. (81) and the algebraic relation (29), the term $m_{mp}\mathbf{r}_{mp} \times \mathbf{a}_{mp}$ in Eq. (80) becomes

$$\begin{aligned} m_{mp}\mathbf{r}_{mp} \times \mathbf{a}_{mp} &= m_{mp}\mathbf{r}_{mp} \times (\dot{\boldsymbol{\omega}}_{mp} \times \mathbf{r}_{mp}) + m_{mp}\mathbf{r}_{mp} \times (\boldsymbol{\omega}_{mp} \times (\boldsymbol{\omega}_{mp} \times \mathbf{r}_{mp})) \\ &= m_{mp}\dot{\boldsymbol{\omega}}_{mp} - m_{mp}(\mathbf{r}_{mp}^T \dot{\boldsymbol{\omega}}_{mp})\mathbf{r}_{mp} - m_{mp}(\mathbf{r}_{mp}^T \boldsymbol{\omega}_{mp})(\boldsymbol{\omega}_{mp} \times \mathbf{r}_{mp}) \end{aligned} \tag{E1}$$

After substituting $\boldsymbol{\omega}_{mp}$ and $\dot{\boldsymbol{\omega}}_{mp}$ from Eqs. (15) and (45), the right-hand side of the above equation will change to

$$\begin{aligned} m_{mp}\mathbf{r}_{mp} \times \mathbf{a}_{mp} =& m_{mp}(\mathbf{J}_{\dot{\omega},mp,1}\ddot{\boldsymbol{\theta}} + \mathbf{J}_{\dot{\omega},mp,2}\dot{\boldsymbol{\theta}}) - m_{mp}(\mathbf{r}_{mp}^T(\mathbf{J}_{\dot{\omega},mp,1}\ddot{\boldsymbol{\theta}} + \mathbf{J}_{\dot{\omega},mp,2}\dot{\boldsymbol{\theta}}))\mathbf{r}_{mp} \\ & - m_{mp}(\mathbf{r}_{mp}^T \mathbf{J}_{mp}\dot{\boldsymbol{\theta}})(\mathbf{J}_{mp}\dot{\boldsymbol{\theta}} \times \mathbf{r}_{mp}) \end{aligned} \tag{E2}$$

Eq. (E2) can be summarized in a matrix form as

$$m_{mp}\mathbf{r}_{mp} \times \mathbf{a}_{mp} = m_{mp}\mathbf{G}_{mp,1}\ddot{\boldsymbol{\theta}} + m_{mp}G_{mp,2}\dot{\boldsymbol{\theta}} \tag{E3}$$

where

$$\mathbf{G}_{mp,1} = \mathbf{J}_{\dot{\omega},mp,1} - \begin{bmatrix} r_{mp,x}\mathbf{r}_{mp}^T \mathbf{J}_{\dot{\omega},mp,1} \\ r_{mp,y}\mathbf{r}_{mp}^T \mathbf{J}_{\dot{\omega},mp,1} \\ r_{mp,z}\mathbf{r}_{mp}^T \mathbf{J}_{\dot{\omega},mp,1} \end{bmatrix} \tag{E4}$$

https://doi.org/10.1017/S026357472100062X Published online by Cambridge University Press

$$\mathbf{G}_{mp,2} = \mathbf{J}_{\dot{\omega},mp,2} - \begin{bmatrix} r_{mp,x}\mathbf{r}_{mp}^T\mathbf{J}_{\dot{\omega},mp,2} \\ r_{mp,y}\mathbf{r}_{mp}^T\mathbf{J}_{\dot{\omega},mp,2} \\ r_{mp,z}\mathbf{r}_{mp}^T\mathbf{J}_{\dot{\omega},mp,2} \end{bmatrix} - \begin{bmatrix} (\mathbf{r}_{mp}^T\mathbf{J}_{mp}\dot{\boldsymbol{\theta}})(r_{mp,z}\mathbf{J}_{mp,2\times(1-3)} - r_{mp,y}\mathbf{J}_{mp,3\times(1-3)}) \\ (\mathbf{r}_{mp}^T\mathbf{J}_{mp}\dot{\boldsymbol{\theta}})(r_{mp,x}\mathbf{J}_{mp,3\times(1-3)} - r_{mp,z}\mathbf{J}_{mp,1\times(1-3)}) \\ (\mathbf{r}_{mp}^T\mathbf{J}_{mp}\dot{\boldsymbol{\theta}})(r_{mp,y}\mathbf{J}_{mp,1\times(1-3)} - r_{mp,x}\mathbf{J}_{mp,2\times(1-3)}) \end{bmatrix} \tag{E5}$$

The above procedure can be easily repeated for other similar terms in Eq. (80) which results in

$$m_{cyl}\mathbf{r}_{cyl,i} \times \mathbf{a}_{cyl,i} = m_{cyl}\mathbf{G}_{cyl,i,1} + m_{cyl}\mathbf{G}_{cyl,i,2} \tag{E6}$$

$$m_{pis}\mathbf{r}_{pis,i} \times \mathbf{a}_{pis,i} = m_{pis}\mathbf{G}_{pis,i,1} + m_{pis}\mathbf{G}_{pis,i,2} \tag{E7}$$

$$m_{pro}\mathbf{r}_{pro,i} \times \mathbf{a}_{cyl,i} = m_{pro}\mathbf{G}_{pro,i,1} + m_{pro}\mathbf{G}_{pro,i,2} \tag{E8}$$

$$m_{dis}\mathbf{r}_{dis,i} \times \mathbf{a}_{dis,i} = m_{dis}\mathbf{G}_{dis,i,1} + m_{dis}\mathbf{G}_{dis,i,2} \tag{E9}$$

where 3×3 matrices $\mathbf{G}_{pro,i,1}$, $\mathbf{G}_{dis,i,1}$, $\mathbf{G}_{cyl,i,1}$ and $\mathbf{G}_{pis,i,1}$ are obtained through replacing subscripts "*mp*" in Eqs. (E4) and (E5) with "*cyl*,*i*", "*pis*,*i*", "*pro*,*i*" and "*dis*,*i*", respectively. Finally, matrices $\mathbf{G}_1$ and $\mathbf{G}_2$are given as

$$\mathbf{G}_1 = -m_{mp}\mathbf{G}_{acc,mp} - m_{pro}\mathbf{G}_{acc,pro,i} - m_{dis}\mathbf{G}_{acc,dis,i} - m_{cyl}\mathbf{G}_{acc,cyl,i} - m_{pis}\mathbf{G}_{acc,pis,i} \tag{E10}$$

$$\mathbf{G}_2 = -m_{mp}\mathbf{G}_{cor,mp} - m_{pro}\mathbf{G}_{cor,pro,i} - m_{dis}\mathbf{G}_{cor,dis,i} - m_{cyl}\mathbf{G}_{cor,cyl,i} - m_{pis}\mathbf{G}_{cor,pis,i} \tag{E11}$$

Appendix F

Unit vector $\mathbf{p}_i = [p_{ix}\ p_{iy}\ p_{iz}]^T$ is located in the plane passing through vectors $\mathbf{u}_i$ and $\mathbf{v}_i$, and also located in the plane passing through vectors $\mathbf{u}_{i+1}$ and $\mathbf{v}_{i+1}$ (Fig. 9), so we can write

$$\mathbf{p}_i^T(\mathbf{u}_i \times \mathbf{v}_i) = 0 \tag{F1}$$

$$\mathbf{p}_i^T(\mathbf{u}_{i+1} \times \mathbf{v}_{i+1}) = 0 \tag{F2}$$

Eqs. (F1) and (F2) can be rewritten as

$$b_1 p_{ix} + b_2 p_{iy} + b_3 p_{iz} = 0 \tag{F3}$$

$$b_4 p_{ix} + b_5 p_{iy} + b_6 p_{iz} = 0 \tag{F4}$$

where

$$\begin{aligned} &b_1 = u_{iy}v_{iz} - u_{iz}v_{iy}, b_2 = -u_{ix}v_{iz} + u_{iz}v_{ix}, b_3 = u_{ix}v_{iy} - u_{iy}v_{ix} \\ &b_4 = u_{i+1,y}v_{i+1,z} - u_{i+1,z}v_{i+1,y}, b_5 = -u_{i+1,x}v_{i+1,z} + u_{i+1,z}v_{i+1,x}, b_6 = u_{i+1,x}v_{i+1,y} - u_{i+1,y}v_{i+1,x} \end{aligned} \tag{F5}$$

Equations (F3) and (F4) constitute a system of two linear equations in three unknowns q_{ix}, q_{iy} and q_{iz}, which can be solved in terms q_{iz} as

$$p_{ix} = \frac{p_{iz}(b_2b_6 - b_3b_5)}{b_1b_5 - b_2b_4} \tag{F6}$$

$$p_{iy} = \frac{p_{iz}(b_3b_4 - b_1b_6)}{b_1b_5 - b_2b_4} \tag{F7}$$

On the other hand, for the unit vector $\mathbf{p}_i$, we have

$$p_{ix}^2 + p_{iy}^2 + p_{iz}^2 = 1 \tag{F8}$$

In this paper, we take $p_{iz} \geq 0$, so Eq. (F8) gives the value of p_{iz}, as

$$p_{iz} = \sqrt{1 - p_{ix}^2 - p_{iy}^2} \tag{F9}$$

With Eqs. (F6), (F7) and (F9), the unique position of vector $\mathbf{p}_i$ is obtained for a given configuration of the manipulator. Subsequently, the smallest angles between $\mathbf{p}_i$ and $\mathbf{u}_i$ and $\mathbf{u}_{i+1}$, that is, α_i' and α_{i+1}', are obtained as

$$\alpha_i' = Arc\cos(\mathbf{p}_i^T\mathbf{u}_i) \tag{F10}$$

$$\alpha_{i+1}' = Arc\cos(\mathbf{p}_i^T\mathbf{u}_{i+1}) \tag{F11}$$

https://doi.org/10.1017/S026357472100062X Published online by Cambridge University Press

Appendix G

Given geometrical properties:

$$\widehat{r}_{mp} = 1 \text{ m}, \widehat{r}_{dis} = 0.92 \text{ m}, t_{mp} = 0.008 \text{ m}, r_{cs} = 0.018 \text{ m}$$
$$l_{cyl} = 0.19 \text{ m}, l_{pis} = 0.21 \text{ m}, \overline{E_i c_{pro,i}} = 0.09 \text{ m}, h = 0.18 \text{ m}$$

and given mass properties:

$$m_{cyl} = 0.4\text{kg}, \bar{\mathbf{I}}_{cyl} = \begin{bmatrix} 0.68 & 0.45 & 0.08 \\ 0.45 & 0.59 & 0.35 \\ 0.08 & 0.35 & 0 \end{bmatrix} \text{kg.m}^2$$

$$m_{pis} = 0.3\text{kg}, \bar{\mathbf{I}}_{pis} = \begin{bmatrix} 0.56 & 0.41 & 0.06 \\ 0.41 & 0.46 & 0.37 \\ 0.06 & 0.37 & 0 \end{bmatrix} \text{kg.m}^2$$

$$m_{pro} = 0.1kg, \bar{\mathbf{r}}_{pro} = [\,0 \quad 0 \quad 0.872\,]^T \text{m}, \bar{\mathbf{I}}_{pro} = \begin{bmatrix} 0.43 & 0.31 & 0 \\ 0.31 & 0.41 & 0.15 \\ 0 & 0.15 & 0.54 \end{bmatrix} \text{kg.m}^2$$

Cite this article: S. Zarkandi (2022). "Task-based torque minimization of a 3-PRR spherical parallel manipulator", Robotica **40**, 475–504. https://doi.org/10.1017/S026357472100062X